Signature of quantum phase transition manifested in quantum fidelity at finite temperature

Protyush Nandi [*]
Department of Physics, University of Calcutta, 92 Acharya Prafulla Chandra Road, Kolkata 700009, India

Sirshendu Bhattacharyya [†]
Department of Physics, Raja Rammohun Roy Mahavidyalaya, Radhanagar, Hooghly 712406, India

Subinay Dasgupta [‡]
Department of Physics, Harish-Chandra Research Institute, Prayagraj 211019, India

(Received 2 February 2023; revised 31 December 2023; accepted 9 February 2024; published 26 February 2024)

The signature of quantum phase transition is generally wiped out at finite temperature. A few quantities that have been observed to carry this signature through a nonanalytic behavior are also limited to low temperatures only. With an aim to identify a suitable dynamical quantity at a high temperature, we have recently constructed a function from quantum fidelity, which has the potential to bear a nonanalytic signature at the quantum critical point beyond low-temperature regime. In this paper, we elaborate our earlier paper and demonstrate the behavior of the corresponding rate function and the robustness of the nonanalyticity for a number of many-body Hamiltonians in different dimensions. We have also shown that our rate function reduces to that used in the demonstration of the dynamical quantum phase transition (DQPT) at zero temperature. It has been further observed that, unlike DQPT, the long-time limit of the rate function can faithfully detect the equilibrium quantum phase transition as well.

DOI: 10.1103/PhysRevB.109.064312

I. INTRODUCTION

Quantum many-body systems, when brought to nonzero temperatures, give rise to interesting dynamical features. In the low-temperature regime, both the quantum and the thermal fluctuations come into play within a quantum critical region. However, the quantum counterpart recedes when we move towards higher temperatures. Therefore, the detection of the phenomena driven by quantum fluctuations, for instance the quantum criticality is generally limited to low temperatures only [1–7]. On the other hand, such detection opens up a new challenge for tracing the imprint of quantum critical phenomena at finite temperatures [8].

Quantum fidelity has been considered to be a powerful tool in the detection of the quantum phase transition (QPT). Defined as a measure of the overlap between the eigenstates of the prequench and postquench Hamiltonians, fidelity can ideally vary from 1 to 0. For a quench across quantum critical point, this value comes close to zero showing a sharp dip because of the structurally different ground states of two phases [9–14]. Different forms of fidelity has been studied at finite temperatures as well [15–22] and some of them have been able to detect the quantum critical point by showing nonanalyticity in their logarithms at low temperatures [15,16].

As the QPT cannot be observed beyond zero temperature, several investigations have been made in search of its trace in different response functions. Quantum coherence has been one of the important functional candidates [23]. At low temperatures, the absorbed energy is reported to be able to detect the quantum critical region [24]. Another related study shows that the expectation values of local order parameters at infinite time exhibiting nonanalytic behavior at critical points at low temperatures [25]. However, it vanishes as the temperature increases. Recently a form of rate function for Loschmidt amplitude studied at finite temperature, has been shown to detect the presence of QPT [26]. The time dependencies of the work distribution function, or the magnetization following quantum quenches or pulses across quantum critical points also bear signatures of QPT [27–32]. Another quantity, the out of time ordered correlations (OTOC) is found to detect quantum critical point through its time averaged form at infinite temperature for 1D ANNNI model [33]. Quantum teleportation protocol applied on 1D XXZ model can also signal quantum critical point at finite temperatures [34,35].

The above findings motivated us to look for a quantity, which will be able to bear signatures of QPT at appreciable temperatures in a d-dimensional system. In an earlier paper, we had defined a form of fidelity in which we could trace down a nonanalytic signature in its rate function at the QCP (quantum critical point) even at high temperatures [36]. At zero temperature, the fidelity reduces to Loschmidt echo, which is used to define dynamical quantum phase transition [27,37–48]. Here in this paper, we extend our earlier study and report a comprehensive extended study on the response of the detector in 1D, 2D, and 3D systems. We confined ourselves to the search for dynamical characteristics at high temperatures.

[*]protyush18@gmail.com
[†]sirs.bh@gmail.com
[‡]subinaydasgupta@hri.res.in

In three dimension, the topological Weyl semimetals have recently emerged as a novel material with unique electronic structures. Here the electrons effectively behave as relativistic Weyl fermions when the Fermi energy is near the crossing points of valence and conduction bands. Unlike topological insulators or topological Dirac semimetals, the Weyl semimetals have broken time reversal symmetry, which leads to a topological phase transition. At zero temperature, Weyl semimetals exhibit a gapped to gapless phase transition. A similar phase transition also occurs in topological nodal line semimetals as well. The only difference between the two is that the Hamiltonian of the Weyl semimetals consists of isolated gapless points in the fermionic momentum space whereas in case of the nodal line semimetals, they form gapless lines. We demonstrate numerically that the rate function mentioned above shows nonanalyticity right at the critical points in both the cases even at finite temperatures.

We also apply our methodology to the quantum spin Hall insulator Bi_4Br_4 using the $k \cdot p$ Hamiltonian proposed for this material [49,50] and find that our (numerically computed) rate function predicts the location of quantum phase transition correctly for this material at low and high temperature.

This paper is organized as follows. In Sec. II we provide the definition of the functional form of the fidelity along with the rate function and derive the expressions for a general d-dimensional system. We study the rate function for one-dimensional XY model in Sec. III and for the 1D Su-Schrieffer-Heeger (SSH) model in Sec. IV. Section V contains the same for the 2D Kitaev model on a honeycomb lattice. The results for 3D systems namely, Weyl semimetal, topological nodal line semimetal and the material Bi_4Br_4 are presented in Sec. VI. In Sec. VII, we discuss the behavior of the detector at zero temperature. This is followed by concluding remarks in Sec. VIII.

II. THEORY

Let us consider a system with Hamiltonian $\mathcal{H}$, dependent on a parameter, which will be quenched from p_0 to p at time $t = 0$ so that the Hamiltonian is quenched from $\mathcal{H}_0 = \mathcal{H}(p_0)$ to $\mathcal{H}' = \mathcal{H}(p)$. We assume that the system was initially in thermal equilibrium at inverse temperature β. We now define quantum fidelity as

$$\mathcal{F}_t \equiv \frac{\mathrm{Tr}[\rho_t \cdot \rho_0]}{\mathrm{Tr}[\rho_t]\,\mathrm{Tr}[\rho_0]} \tag{1}$$

where ρ_0 is the density matrix at $t = 0$ and ρ_t is the same after the system has evolved through time t,

$$\begin{aligned} \rho_0 &= \exp(-\beta\mathcal{H}_0), \\ \rho_t &= \exp(-i\mathcal{H}'t)\exp(-\beta\mathcal{H}_0)\exp(i\mathcal{H}'t). \end{aligned} \tag{2}$$

One may note that the probability of overlap between initial and time-evolved states namely $|\langle\psi(0)|\psi(t)\rangle|^2$, is known as the Loschmidt echo, which shows nonanalytic kinks in its logarithm as a function of time when the Hamiltonian is quenched across a QCP [51]. Our expression for fidelity reduces to this Loschmidt echo, when brought to zero temperature. We may define a measurable quantity called rate function as

$$r(t, \beta, p_0, p) \equiv -\lim_{N\to\infty} \frac{1}{N} \log \mathcal{F}_t \tag{3}$$

where N is the system size. The quantity of our interest is the long-time average of this rate function, defined as

$$r_a(\beta, p_0, p) \equiv \lim_{\tau\to\infty} \frac{1}{\tau} \int_0^\tau r(t, \beta, p_0, p)\, dt. \tag{4}$$

This is the detector we shall use to locate the presence of QCP at a finite temperature. We shall investigate if the behavior of

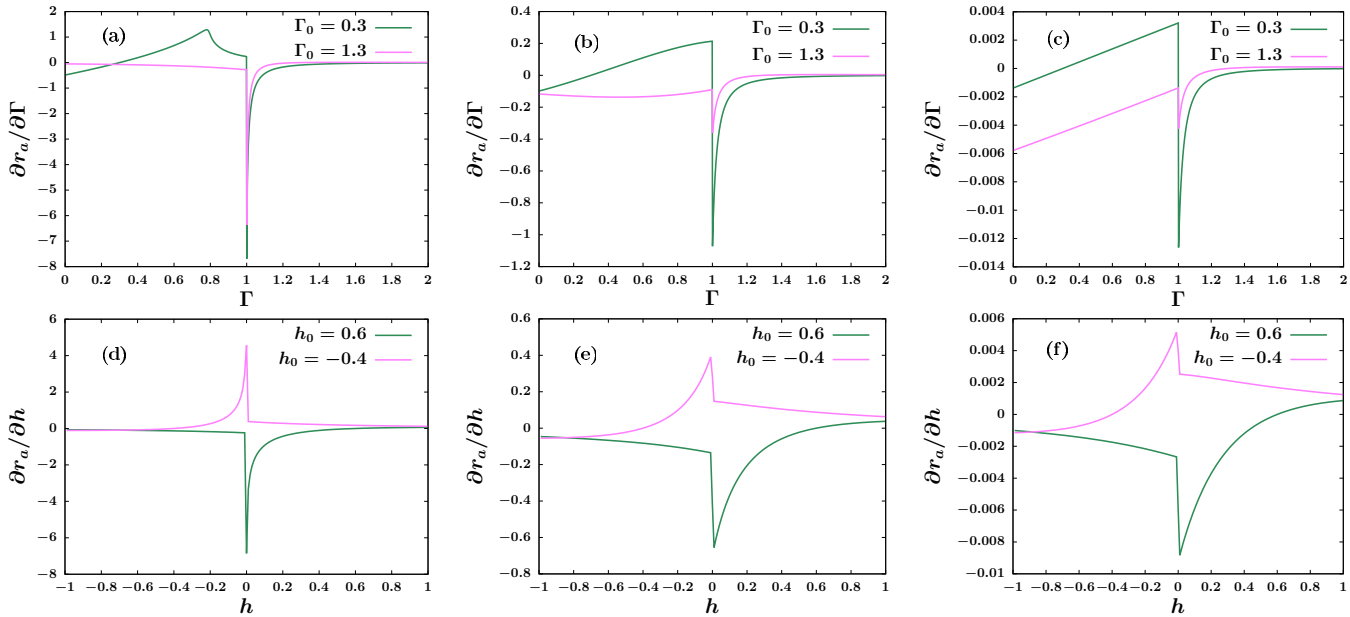

FIG. 1. Transverse XY chain. First derivative of rate function with respect to the quench parameter, computed numerically for quench of transverse field parameter Γ for $h = 0.3$ at (a) $\beta = 10$, (b) $\beta = 1$, and (c) $\beta = 0.1$ and for quench of anisotropy parameter h for $\Gamma = 0.3$ at (d) $\beta = 10$, (e) $\beta = 1$, and (f) $\beta = 0.1$ In both cases the quantity $\partial r_a/\partial\Gamma$ is discontinuous at the critical point $\Gamma = 1$ and $h = 0$.

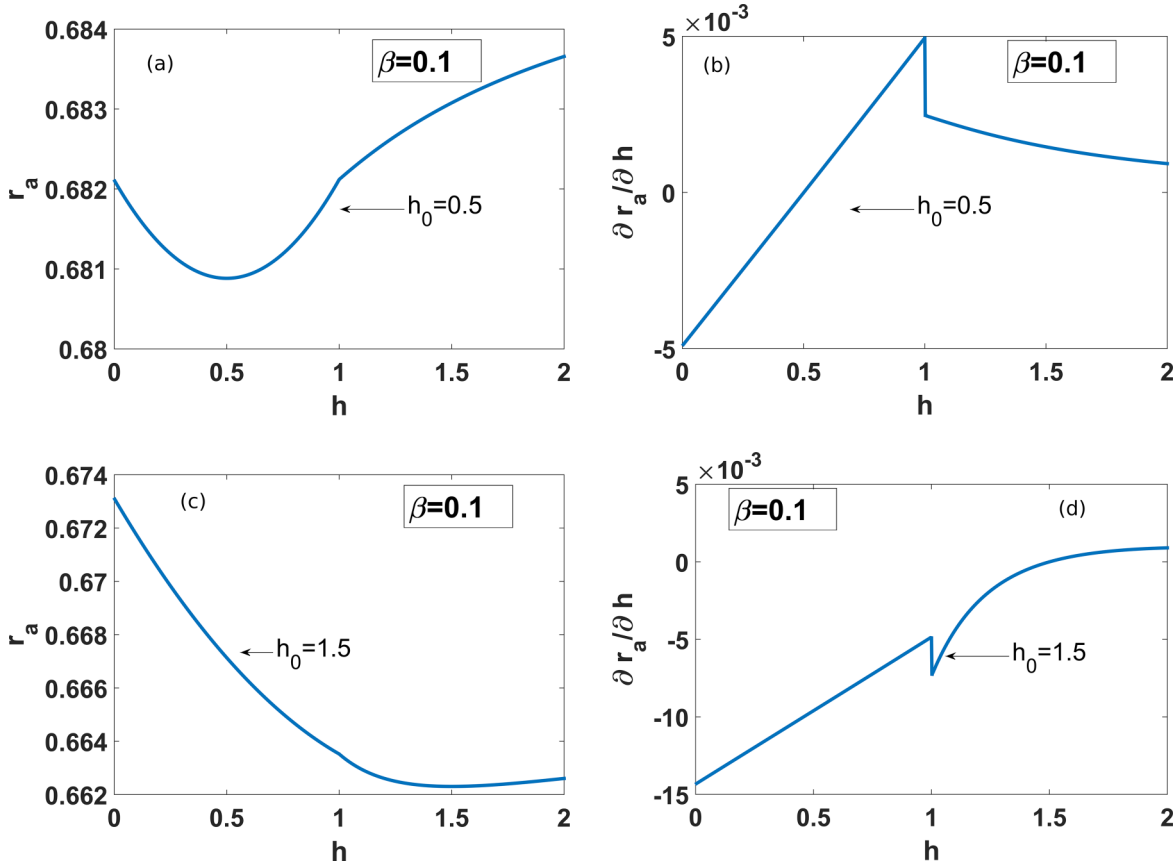

FIG. 2. 1D SSH model. The plots are the rate function and derivative of rate function with respect to postquench parameter h for $h_0 = 0.5$ in (a) and (b) and $h_0 = 1.5$ in (c) and (d) at inverse temperature $\beta = 0.1$.

this quantity, at zero and nonzero temperatures bears a signature of QCP. In order to study this rate function we consider a class of systems with a generic Hamiltonian expressible as a sum of commuting 2×2 Hamiltonians in the space of wave vectors $\vec{q}$

$$\mathcal{H} = \sum_{\vec{q}} \mathcal{H}_{\vec{q}} \tag{5}$$

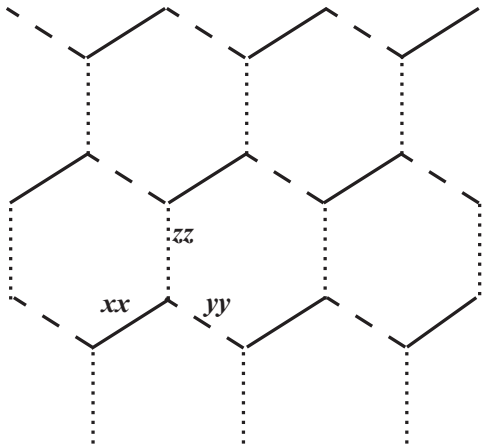

FIG. 3. Kitaev model on honeycomb lattice. The continuous, dashed, and dotted lines correspond to xx, yy, and zz interactions, with interaction strengths J_1, J_2, J_3 respectively.

and express $\mathcal{H}_{\vec{q}}$ as

$$\mathcal{H}_{\vec{q}} = a_{\vec{q}}\sigma_1 + b_{\vec{q}}\sigma_2 + c_{\vec{q}}\sigma_3 = \lambda_{\vec{q}}(\hat{\mathcal{V}}_{\vec{q}} \cdot \vec{\sigma}). \tag{6}$$

Here σ_i are the Pauli spin matrices, $\lambda_{\vec{q}} = \sqrt{a_{\vec{q}}^2 + b_{\vec{q}}^2 + c_{\vec{q}}^2}$, $\hat{\mathcal{V}}_{\vec{q}} = (a_{\vec{q}}/\lambda_{\vec{q}}, b_{\vec{q}}/\lambda_{\vec{q}}, c_{\vec{q}}/\lambda_{\vec{q}})$ where $\vec{q}$ is d-dimensional wave vector. After quenching $p_0 \to p$, the Hamiltonian becomes

$$\mathcal{H}'_{\vec{q}} = \mathcal{H}_{\vec{q}}(p) = \lambda'_{\vec{q}}(\mathcal{V}'_{\vec{q}} \cdot \vec{\sigma}).$$

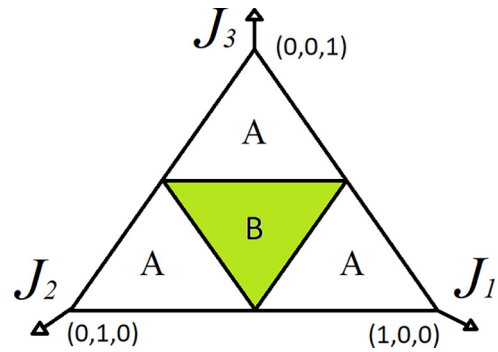

FIG. 4. The phase diagram of Kitaev model in honeycomb lattice. The regions marked A are gapped regions and B is the gapless region [63].

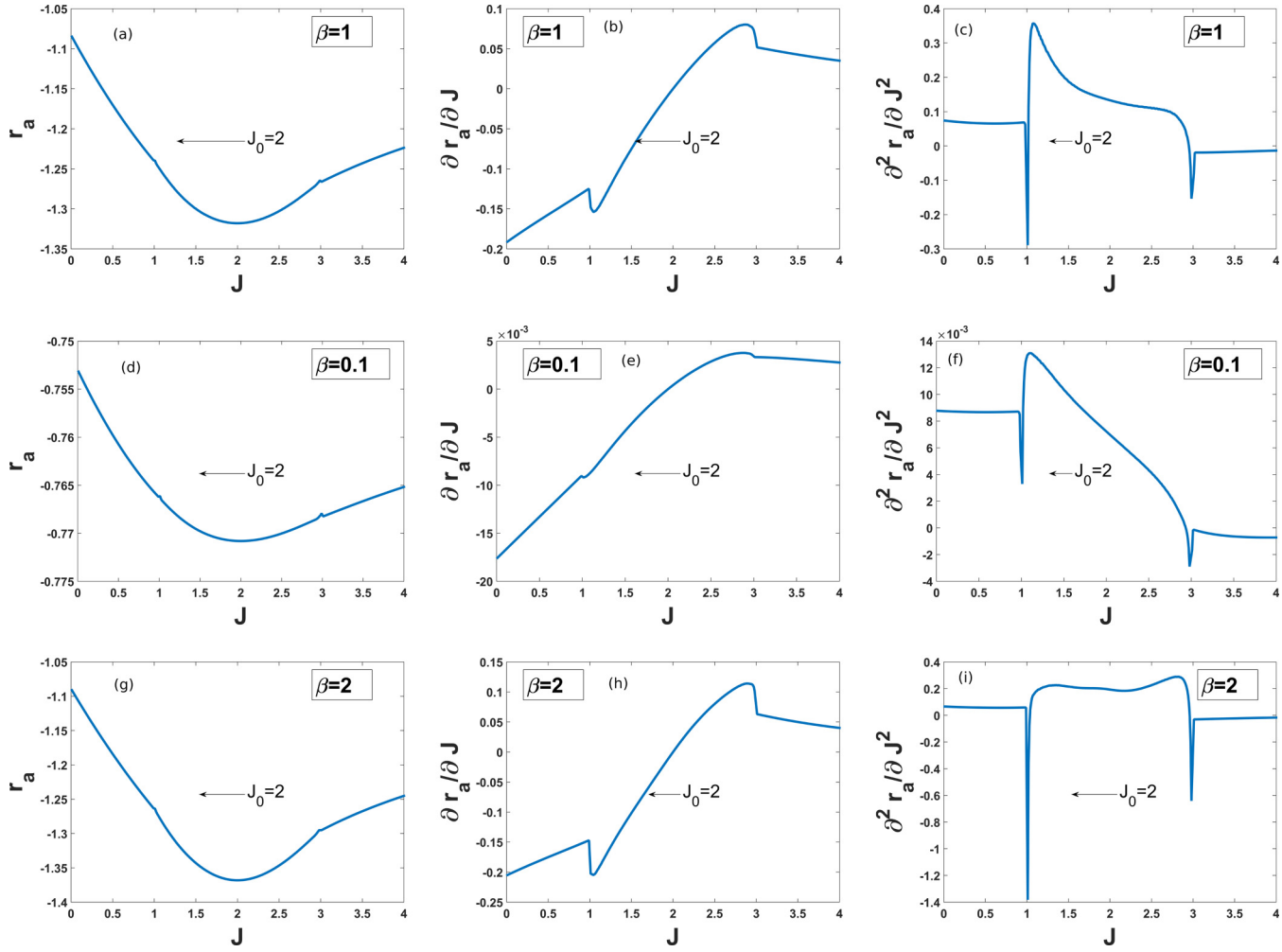

FIG. 5. Kitaev model on honeycomb lattice. Plots of r_a, $\partial r_a/\partial J$, $\partial^2 r_a/\partial J^2$ vs J. We have fixed $J_1 = 2$ and $J_2 = 1$. We have plotted for three different temperatures $\beta = 1$ in (a), (b), and (c), $\beta = 0.1$ in (c), (d), and (e) and $\beta = 2$ in (g), (h), and (i). The initial value of J_3 is $J_0 = 2$. It is evident from the plots that the rate function is showing nonanalyticities at QCPs at $J = 1$ and $J = 3$.

Here $\lambda'_{\vec{q}} = \sqrt{a'^2_{\vec{q}} + b'^2_{\vec{q}} + c'^2_{\vec{q}}}$, $\hat{\mathcal{V}}'_{\vec{q}} = (a'_{\vec{q}}/\lambda'_{\vec{q}}, b'_{\vec{q}}/\lambda'_{\vec{q}}, c'_{\vec{q}}/\lambda'_{\vec{q}})$ and the primed quantities are the postquench values. We can calculate the exponentials in ρ_0 and ρ_t by exploiting the property that

$$\mathcal{H}^2_{\vec{q}} = \lambda^2_{\vec{q}} \underline{1} \quad \text{and} \quad \mathcal{H}'^2_{\vec{q}} = \lambda'^2_{\vec{q}} \underline{1},$$

$(\hat{\mathcal{V}}_{\vec{q}} \cdot \vec{\sigma})^2 = 1$ and obtain the fidelity in Eq. (1) as

$$\mathcal{F}_t(t, \beta, p_0, p) = \tfrac{1}{2}\big(1 + \tanh^2(\beta\lambda_{\vec{q}}) \times [1 - 2\sin^2(\lambda'_{\vec{q}}t)\{1 - (\hat{\mathcal{V}}'_{\vec{q}}.\hat{\mathcal{V}}_{\vec{q}})^2\}]\big). \quad (7)$$

Hence the rate function (3) of the generic Hamiltonian (5) can be written as

$$r(t, \beta, p_0, p) = \log 2 - \frac{1}{V}\int_{\vec{q}} d\vec{q}\ \log \times [1 + \tanh^2(\beta\lambda_{\vec{q}})\{1 - 2\sin^2(\lambda'_{\vec{q}}t)\,\mathcal{L}_{\vec{q}}\}] \quad (8)$$

in d dimensions where the volume of the d-dimensional first Brillouin zone is written as $V = \int_{\vec{q}} d\vec{q}$, $\mathcal{L}_{\vec{q}} = 1 - (\hat{\mathcal{V}}_{\vec{q}} \cdot \hat{\mathcal{V}}'_{\vec{q}})^2 = \sin^2(\phi_{\vec{q}})$, $\phi_{\vec{q}}$ is the angle between $\hat{\mathcal{V}}_{\vec{q}}$ and $\hat{\mathcal{V}}'_{\vec{q}}$. We can calculate the long-time average of the rate function from the Eq. (4) using standard results [52],

$$r_a(\beta, p_0, p) = 3\log 2 - \frac{1}{V}\int_{\vec{q}} \log(1 + \alpha_{\vec{q}})d\vec{q} - \frac{2}{V}\int_{\vec{q}} \log[1 + \sqrt{1 - \gamma_{\vec{q}}\mathcal{L}_{\vec{q}}}]d\vec{q} \quad (9)$$

where $\alpha_{\vec{q}} = \tanh^2(\beta\lambda_{\vec{q}})$, $\gamma_{\vec{q}} = 2\alpha_{\vec{q}}/(1 + \alpha_{\vec{q}}) = 1 - \text{sech}(2\beta\lambda_{\vec{q}})$.

Since both $\gamma_{\vec{q}}$ and $\mathcal{L}_{\vec{q}}$ have values between 0 and 1, we can expand the integrand in the third term of Eq. (9),

$$r_a(\beta, p_0, p) = \log 2 - \frac{1}{V}\int_{\vec{q}} \log(1 + \alpha_{\vec{q}})d\vec{q} + \frac{1}{2V}\sum_{n=1}^{\infty} c_n \int_{\vec{q}} \gamma^n_{\vec{q}}\mathcal{L}^n_{\vec{q}}d\vec{q} \quad (10)$$

where c_n are constants generated from the expansion and $c_1 = 1, c_2 = \frac{3}{8}, c_3 = \frac{5}{24}$ etc. For detailed derivation of Eqs. (8), (9), and (10), see Appendix A. Our objective is to study the quantity $r_a(\beta, p_0, p)$ as a function of the postquench value p of this parameter. Actually we shall look for nonanalytic behavior of the quantities $\partial r_a(\beta, p_0, p)/\partial p$ and/or

$\partial^2 r_a(\beta, p_0, p)/\partial p^2$. While differentiating Eq. (10), the first two terms become zero as they are not functions of p. Therefore the third term is our subject of interest.

For all the Hamiltonians considered below, we have verified numerically that the predominant contribution to the nonanalytic behavior (if any) in the double derivative comes from the point (called node) where $\lambda'_{\vec{q}}$ becomes zero. Therefore, in the second integral in Eq. (10), $\lambda_{\vec{q}}$ and $\gamma_{\vec{q}}$ are brought out of the integral by replacing $\lambda_{\vec{q}}$ by its value at the node. So we can write

$$r_a(\beta, p_0, p) = \log 2 - \frac{1}{V}\int \log(1+\alpha_{\vec{q}})d\vec{q} + \frac{1}{2V}\sum_n c_n \frac{\gamma^n}{\lambda^{2n}} I_n \tag{11}$$

where λ and γ are the value of $\lambda_{\vec{q}}$ and $\gamma_{\vec{q}}$ at the node, and

$$I_n(p_0, p) = \int_{\vec{q}} \lambda_{\vec{q}}{}^{2n} \mathcal{L}_{\vec{q}}{}^n \, d\vec{q}.$$

Following our earlier paper [36], we shall show below that the nonanalyticity comes from the integral I_n and since I_n is independent of temperature, the signature of the existence of QCP is expected to show up at all temperatures.

We shall apply the above prescription to several integrable quantum spin models, namely the XY chain, 1D SSH model, the Kitaev model on a honeycomb lattice, Weyl semimetals, and topological nodal line semimetals. Each of these models shows a QCP at absolute zero temperature. We shall show that the quantity r_a shows a nonanalytic behavior at the QCP at *any* finite temperature. Indeed, it does not imply that there is *actually* a phase transition at a finite temperature but that the detector, namely, the long-time fidelity, bears a signature of criticality, which exists at zero temperature. Furthermore, since the evaluation of the relevant quantity only involves the evaluation of an integral, we can study numerically the three-dimensional systems also. We shall report that for Weyl semimetals and topological nodal line semimetals, at low temperatures the long-time fidelity shows nonanalytic behavior at the phase boundary.

III. TRANSVERSE FIELD XY MODEL

The XY model in 1D is defined by

$$\mathcal{H}_{XY} = -\frac{1}{2}(1+h)\sum_{i=1}^{N} s_i^x s_{i+1}^x - \frac{1}{2}(1-h)\sum_{i=1}^{N} s_i^y s_{i+1}^y - \Gamma\sum_{i=1}^{N} s_i^z \tag{12}$$

where h is the anisotropy parameter and Γ is the transverse field and s_i are Pauli matrices. One can show by using Jordan-Wigner transformation [1,53,54] that this Hamiltonian can be written in the form of Eq. (5), where

$$\mathcal{H}_q = a_q\sigma_1 + b_q\sigma_3. \tag{13}$$

Here $a_q = -h\sin(q)$ and $b_q = \Gamma + \cos(q)$ with $0 < q < \pi$. There is a disordered phase in the region $|\Gamma| > 1$ and two ordered phases for $h > 0$, $|\Gamma| < 1$ and $h < 0$, $|\Gamma| < 1$.

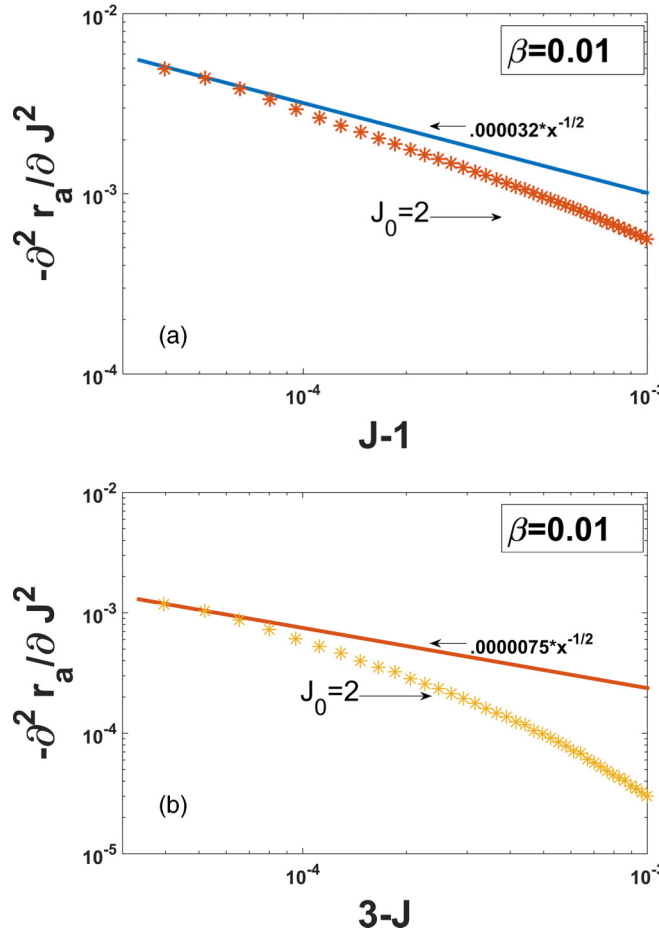

FIG. 6. Kitaev model on honeycomb lattice. (a) $-\partial^2 r_a/\partial J$ vs $J-1$ is plotted for $J_1 = 2$ and $J_2 = 1$. As it approaches critical point $J = 1$, it coincides with the blue line, which diverges as $x^{-1/2}$. (b) $-\partial^2 r_a/\partial J^2$ vs $3-J$ is plotted. As it approaches critical point $J = 3$, it starts diverging as $x^{-1/2}$.

The long-time average of the rate function is now given by Eq. (9) with $\vec{q}$ as a scalar. We will study two quench protocols, one for the quench of external field (Γ) and the other for quench of the anisotropy parameter (h).

A. Quench of external field

We quench Γ instantaneously from some initial value Γ_0 to Γ keeping h constant. The derivative $\partial r_a/\partial\Gamma$, calculated numerically shows a discontinuity at $\Gamma = 1$, which is the quantum critical point at the temperature $T = 0$ (Fig. 1). This proves that our detector r_a can successfully detect the QCP even at a large temperature as we have reported in our previous paper [36].

We can also derive an analytic expression for the amount of discontinuity at high temperatures from Eq. (9). The parameter p becomes Γ in this case, V becomes π as the system is one-dimensional and q ranges from 0 to π. The quantity $\mathcal{L}_q$ becomes

$$\mathcal{L}_q = (\Gamma - \Gamma_0)^2\left(\frac{a_q}{\lambda_q\lambda'_q}\right)^2.$$

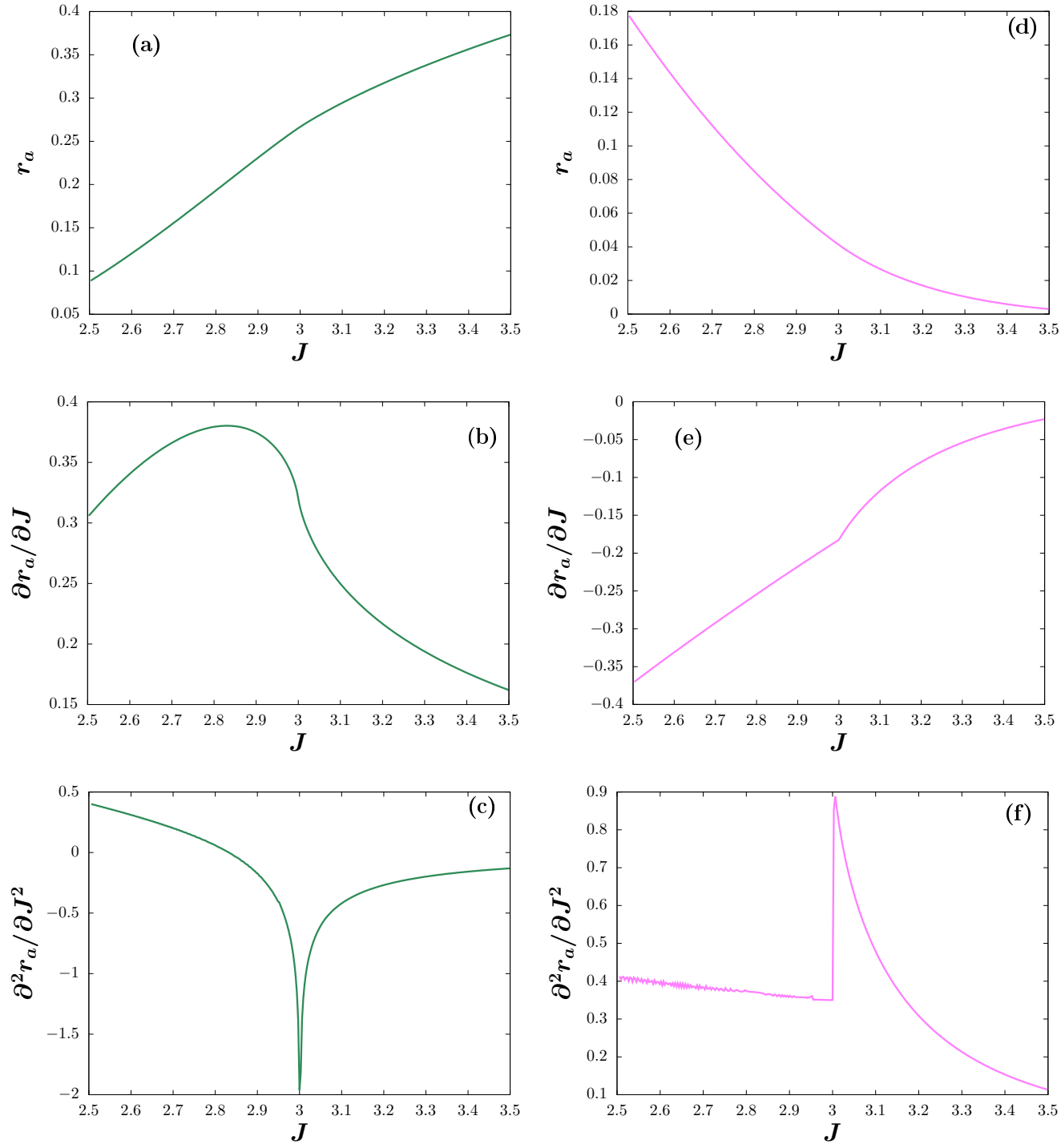

FIG. 7. 3D Weyl semimetal. Rate function r_a and its two derivatives computed numerically from Eqs. (9) for quench of the parameter $J_0 \to J$ at $\beta = 4$. For (a), (b), and (c), the prequench value is within the gapless phase $J_0 = 2$, while for (d), (e), and (f) it is within the gapped phase $J_0 = 3.8$. In both cases the quantity $\partial^2 r_a/\partial J^2$ diverges at the phase boundary $J = 3$.

Following Eq. (11) we express I_n as

$$I_n = (\Gamma - \Gamma_0)^{2n} \int_0^{\pi} \left(\frac{a_q}{\lambda_q'}\right)^{2n} dq. \tag{14}$$

For $n = 1$, one can calculate the integral directly,

$$I_1 = \frac{\pi}{4}(\Gamma - \Gamma_0)^2\left(1 + \frac{1}{\Gamma^4}\right) \quad \text{for } \Gamma > 1 \tag{15}$$

and

$$I_1 = \frac{\pi}{4}(\Gamma - \Gamma_0)^2\left(\Gamma^2 + \frac{1}{\Gamma^2}\right) \quad \text{for } \Gamma < 1. \tag{16}$$

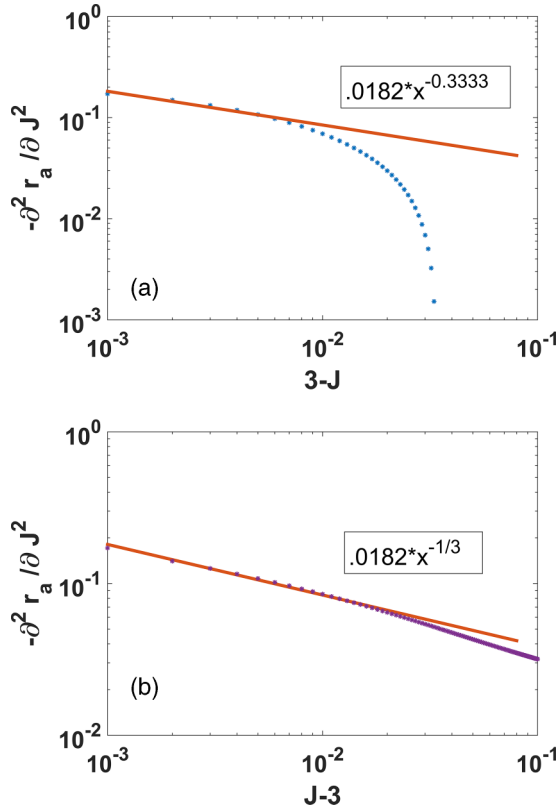

FIG. 8. 3D Weyl semimetal. (a) $-\partial^2 r_a/\partial J$ vs J is plotted very close to the quantum critical point at $J = 3$. It is evident from the figure that double derivative diverges algebraically both from left (a) and from right (b) of the critical point with a critical exponent $-1/3$.

When the temperature is high, β is small and I_1 is the most dominant term (refer to Appendix C). The amount of discontinuity at the QCP $\Gamma = 1$ is then

$$(\partial r_a/\partial\Gamma)_{\Gamma=1+} - (\partial r_a/\partial\Gamma)_{\Gamma=1-} = \beta^2\left(1-\Gamma_0^2\right)/h. \quad (17)$$

At high temperatures, we have calculated numerically the discontinuity in $\partial r_a/\partial\Gamma$ keeping all values of n, and found the result to be of the same order of magnitude as that obtained by keeping the $n = 1$ term only (refer to Appendix C).

B. Quench of anisotropy parameter

In this case, we quench h instantaneously from some initial value h_0 to h keeping Γ constant. The derivative $\partial r_a/\partial h$, calculated numerically shows a discontinuity at the phase boundary $h = 0$ (Fig. 1). Thus, here also our detector r_a can successfully detect the QCP even at a large temperature as we have reported in our previous paper [36].

The parameter p of Eq. (9) becomes h in this case and V becomes π for the reason mentioned in the previous subsection. $\mathcal{L}_q$ then becomes

$$\mathcal{L}_q = (h-h_0)^2\left(\frac{b_q'\sin(q)}{\lambda_q'\lambda_q}\right)^2.$$

We write the integral in the third term of Eq. (11) as

$$I_n = (h-h_0)^{2n}\int\left(\frac{b_q'\sin(q)}{\lambda_q'}\right)^{2n} dq. \quad (18)$$

The term I_1 can be obtained as

$$I_1 = -\frac{\pi}{4}(h-h_0)^2\{6h^2(2\Gamma^2-1)+4h(\Gamma^2-1)-2\} \quad \text{for } h<0 \quad (19)$$

and

$$I_1 = -\frac{\pi}{4}(h-h_0)^2\{2h^2(4\Gamma^2-1)-4h(\Gamma^2-1)-2\} \quad \text{for } h>0. \quad (20)$$

This gives the amount of discontinuity at the QCP $h = 0$ at high temperatures as

$$(\partial r_a/\partial h)_{h=0+} - (\partial r_a/\partial h)_{h=0-} = 2\beta^2 h_0^2(1-\Gamma^2). \quad (21)$$

As before, the discontinuity calculated by keeping all values of n turns out to be of the same order of magnitude as that obtained by keeping the $n = 1$ term only (refer to Appendix C).

IV. 1D SSH MODEL

The Su-Schrieffer-Heeger (SSH) model can be thought of as a chain of N unit cells with each unit cell consisting of two different sites labeled as c and d [55,56]. The Hamiltonian in position space can be written as

$$\mathcal{H} = -\sum_n [c_n^\dagger d_n + h c_{n+1}^\dagger d_n + \text{H.c}] \quad (22)$$

where c_n and d_n are the fermionic annihilation operators at site c and site d respectively at the nth unit cell and $c^\dagger$, $d^\dagger$ are the corresponding creation operators. After Fourier transformation, the Hamiltonian is transformed into the form of Eq. (5),

$$\mathcal{H} = \sum_q \mathcal{H}_q \quad \text{where} \quad \mathcal{H}_q = a_q\sigma_1 + b_q\sigma_2 \quad (23)$$

with $a_q = (1 + h\cos(q))$ and $b_q = h\sin(q)$ where q ranges from $-\pi$ to π. This model shows phase transition at $h = \pm 1$.

The parameter h is quenched from h_0 to h and the system is allowed to evolve. Using Eq. (9), one can calculate numerically the rate function r_a and its derivatives $\partial r_a/\partial h$. One finds (Fig. 2) a discontinuity in $\partial r_a/\partial h$ at $h = 1$, which shows that the r_a detects the QCP even at finite temperatures. We can analytically calculate the amount of discontinuity in $\partial r_a/\partial h$ at the QCP. The quantity p becomes h in this case, V is equal to 2π and $\mathcal{L}_q$ is

$$\mathcal{L}_q = \left(\frac{a_q b_q' - b_q a_q'}{\lambda_q\lambda_q'}\right)^2 \quad (24)$$

with the primed quantities being the postquench parameters.

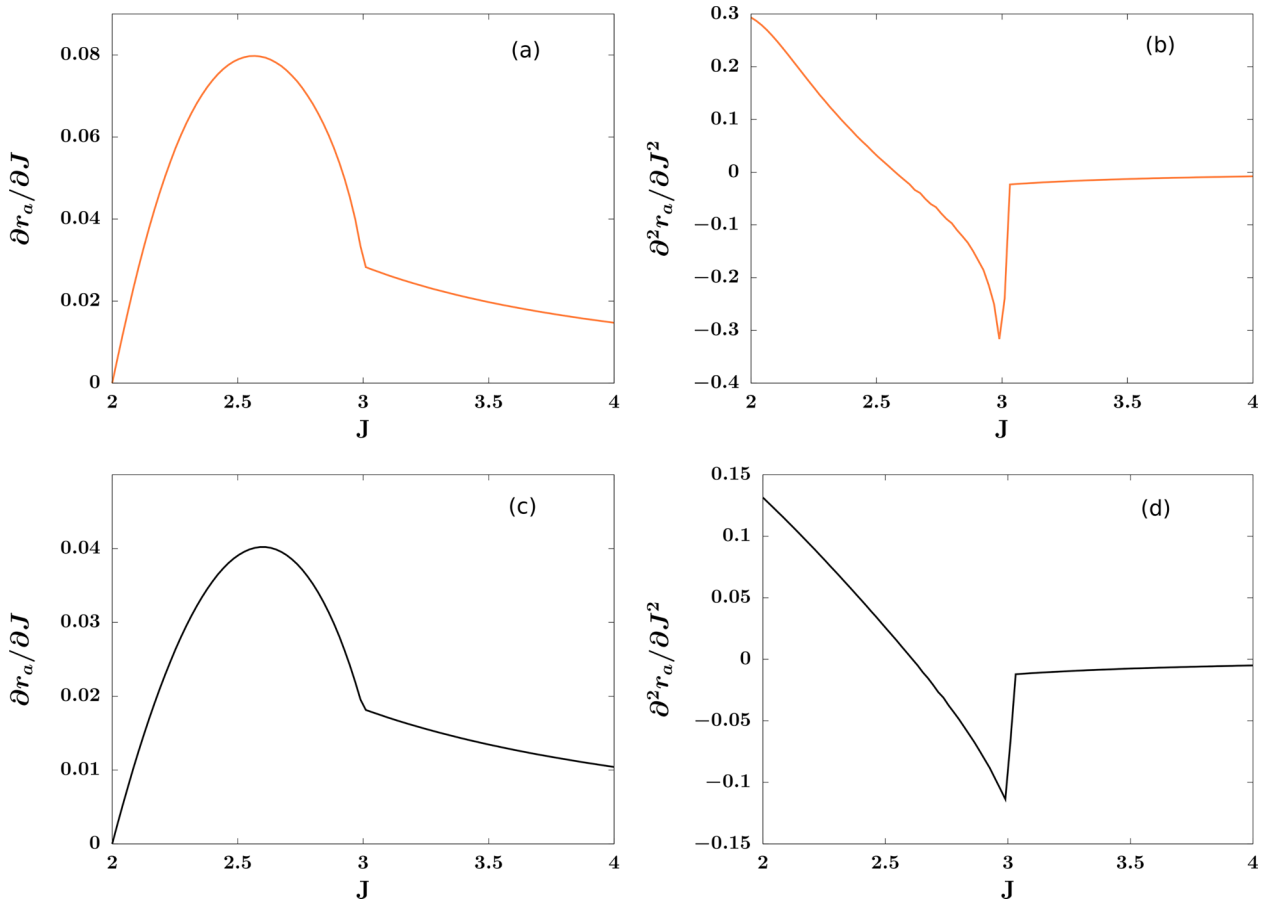

FIG. 9. 3D topological nodal line semimetal. First and second derivatives of the rate function computed numerically from Eqs. (9) for quench of the parameter $J_0 = 2 \to J$ at $\beta = 4$ [(a) and (b)] and $\beta = 1$ [(c) and (d)]. In both cases the quantity $\partial^2 r_a/\partial J^2$ is discontinuous at the phase boundary $J = 3$.

We can now write the integral in the the third term of Eq. (11) as

$$I_n = \int_{q=-\pi}^{\pi} \left(\frac{a_q b'_q - b_q a'_q}{\lambda'_q}\right)^{2n} dq$$
$$= (h-h_0)^{2n} \int_{q=-\pi}^{\pi} \left(\frac{\sin^2(q)}{1+h^2+2h\sin(q)}\right)^{n} dq. \quad (25)$$

At high temperature, the most dominant contribution comes from I_1, which can be calculated easily,

$$I_1 = \pi(h-h_0)^2 \quad \text{for } h < 1 \quad (26)$$

and

$$I_1 = \pi \frac{(h-h_0)^2}{h^2} \quad \text{for } h > 1. \quad (27)$$

Hence, the amount of discontinuity in the first derivative of r_a at $h = 1$ (at high temperature) is

$$\partial r_a/\partial h|_{h=1+} - \partial r_a/\partial h|_{h=1-} = -2\beta^2(h_0-1)^2. \quad (28)$$

As before, the discontinuity calculated by keeping all values of n turns out to be of the same order of magnitude as that obtained by keeping the $n = 1$ term only (refer to Appendix C).

V. TWO-DIMENSIONAL CASE: KITAEV MODEL

The Hamiltonian of the Kitaev model on a honeycomb lattice is defined as

$$\mathcal{H} = \sum_{i,j} \sum_{\alpha=1}^{3} J_\alpha \sigma_i^\alpha \sigma_j^\alpha \quad (29)$$

where i, j run over all the nearest-neighboring pairs on the lattice. This model contains three interaction parameters $J_{1,2,3}$ (Fig. 3). It can be shown [57–59] that in the "vortex-free" sector this Hamiltonian can again be written like Eq. (5) with

$$\mathcal{H}_{\vec{q}} = a_{\vec{q}}\sigma_1 + b_{\vec{q}}\sigma_3. \quad (30)$$

Here $\vec{q} = (q_x, q_y)$ where $-\pi < (q_x, q_y) < \pi$ and the coefficients are [60,61]

$$a_{\vec{q}} = -J_1 \sin(q_x) + J_2 \sin(q_y),$$
$$b_{\vec{q}} = J_3 - J_1 \cos(q_x) - J_2 \cos(q_y). \quad (31)$$

The phase diagram of the system in the vortex free state is given in Fig. 4. There is a gapless region for the parameter values satisfying the inequality $|J_1 - J_2| \leqslant J_3 \leqslant J_1 + J_2$ and a gapped region elsewhere. These two phases are topologically different [57–59] and cannot always be detected by studying Loschmidt echo [62].

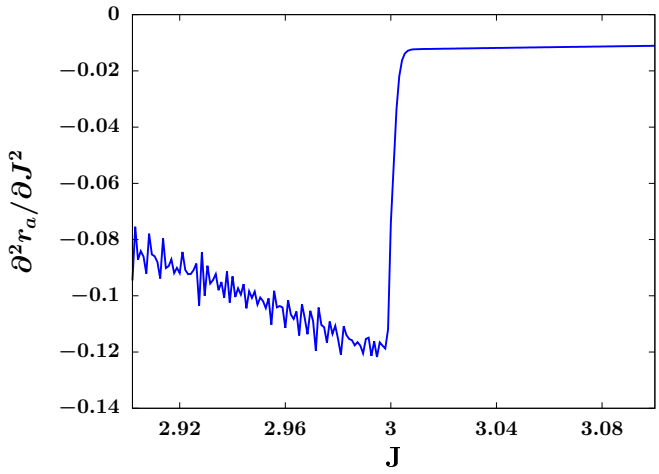

FIG. 10. 3D topological nodal line semimetal. Double derivative with respect to J vs J is plotted very close to the quantum critical point at J = 3 for $\beta = 1$ and $J_0 = 2$. It is evident from the figure that there is a finite discontinuity. The reason behind the oscillation in the curve is computational limitation.

We have dealt with the case where $J_1 = J_2$ in our previous paper [36]. Here we will deal with the more general case of $J_1 \neq J_2$. Using Eq. (9), one can calculate numerically the rate function and its derivatives for quench of the parameter J_3 for a fixed J_1 and J_2 (Fig. 5). We find that a nonanalyticity occurs at $|J_1 - J_2|$ and $J_1 + J_2$ and that the double derivative of the rate function diverges with a critical exponent of 1/2 (Fig. 6).

We shall now present an analytic treatment for the case $J_1 \neq J_2$ for a quench of J_3 from J_0 to J. Here, the parameter p is J, V is $4\pi^2$ and $\mathcal{L}_{\vec{q}}$ can be written as

$$\mathcal{L}_{\vec{q}} = (J - J_0)^2 \frac{a'^2_{\vec{q}}}{\lambda^2_{\vec{q}}\, \lambda'^2_{\vec{q}}}.$$

We substitute

$$M = J_1 + J_2, \quad N = J_1 - J_2, \quad u = \frac{q_x + q_y}{2}, \quad v = \frac{q_x - q_y}{2}$$

to get

$$a_{\vec{q}} = -M\cos(u)\sin(v) - N\sin(u)\cos(v),$$
$$b_{\vec{q}} = J_3 - M\cos(u)\cos(v) + N\sin(u)\sin(v). \quad (32)$$

We can now write the the expression of r_a from Eq. (11). Since only the third term will remain after the differentiation with respect to J, we will calculate the integrand in the third term of the rate function, namely,

$$I_n = 4(J - J_0)^{2n} \int_{u=0}^{\pi/2} du \int_{v=-\pi}^{\pi} dv \left(\frac{a'}{\lambda'}\right)^{2n}. \quad (33)$$

The analytic expression of I_1 is obtained as (see Appendix B)

$$I_1 = \frac{2\pi}{J}(J - J_0)^2 \Bigg[2Ju_c - (M^2 - N^2)\frac{\sin(2u_c)}{2J} + \frac{1}{J}(M^2 + N^2)\left(\frac{\pi}{2} - u_c\right)\Bigg] \quad (34)$$

where $u_c = \cos^{-1}\left(\sqrt{(J^2 - N^2)/(M^2 - N^2)}\right)$. If we approach $|N|$ from the gapless phase and approximate J close to $|N|$ as

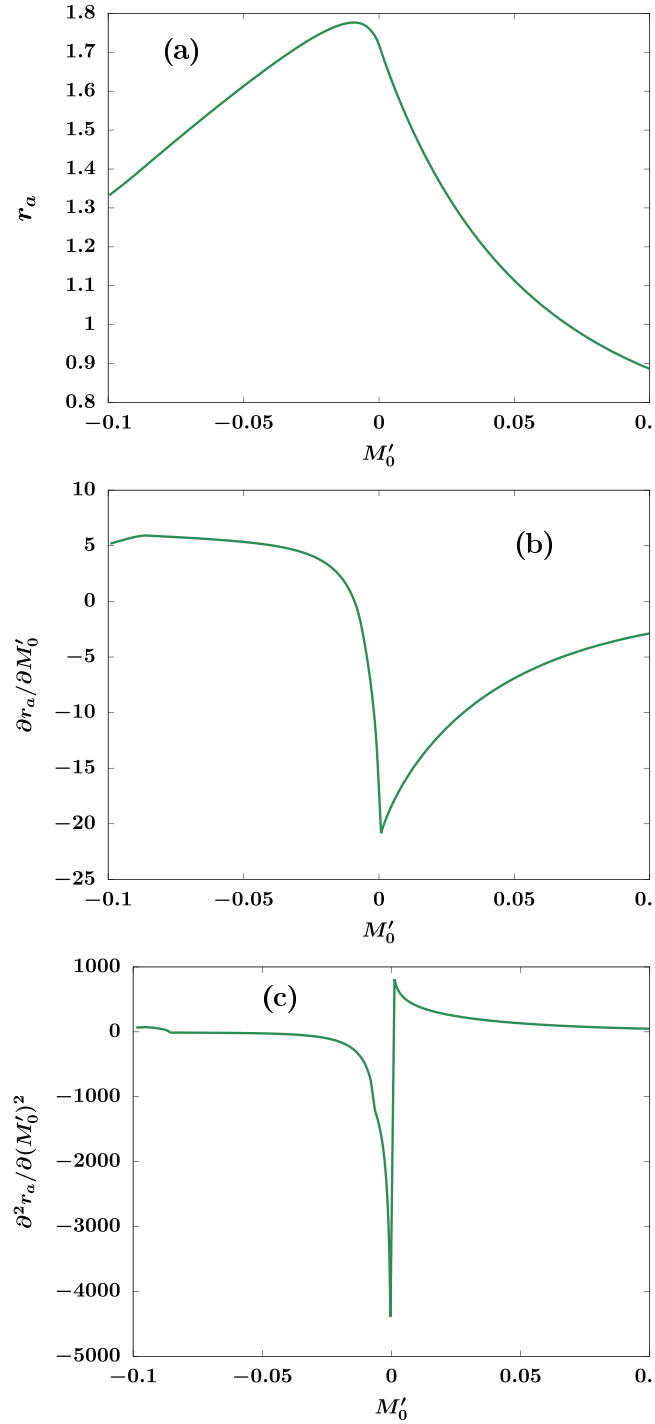

FIG. 11. Rate function r_a (a) and its first (b) and second (c) derivatives are plotted against M_0' for room temperature. Since we have used a $k.p$ Hamiltonian, the integration is done on a region close to the center of the Brillouin zone, namely, $0.05\ \text{Å}^{-1} \leqslant q_x, q_y \leqslant 0.05\ \text{Å}^{-1}$ following [49].

$|N| + \epsilon$, we obtain

$$\frac{\partial^2 I_1}{\partial J^2} = -\frac{4\pi\sqrt{2}(|N| - J_0)^2}{\sqrt{|N|(M^2 - N^2)}}\epsilon^{-1/2} \quad (35)$$

up to leading order.

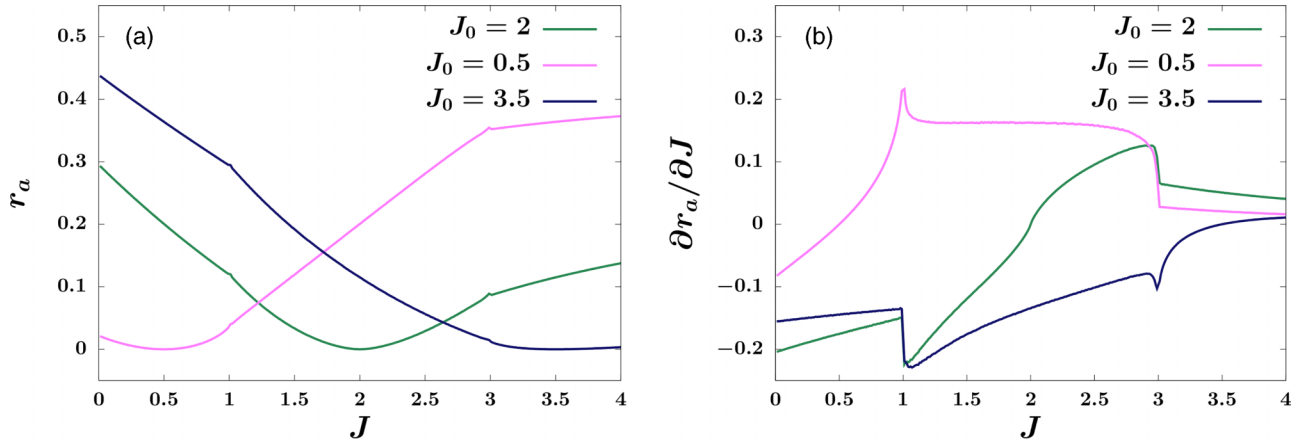

FIG. 12. Rate function r_a (a) and its derivative (b) for 2D Kitaev Model computed from Eq. (46) at zero temperature with the prequench parameter $J_0 = 2$ (in gapless phase), $J_0 = 0.5$ and $J_0 = 3.5$ (in gapped phase). Nonanalyticity appears only at the phase boundary $J = 3$ and $J = 1$.

In the same way, we can show that if we approach M from the gapless phase and approximate J close to M as $M - \epsilon$,

$$\frac{\partial^2 I_1}{\partial J^2} = -\frac{4\pi\sqrt{2}(M - J_0)^2}{\sqrt{M(M^2 - N^2)}}\epsilon^{-1/2} \tag{36}$$

up to leading order.

We conclude that the double derivative of I_n will also be proportional to $\epsilon^{-1/2}$ up to the leading order. Hence, the double derivative of r_a diverges algebraically with the exponent $1/2$ near both the critical points at any temperature (Fig. 6). Although we have not considered vortex excitation in the nonzero temperature, the excitation of vortices does not destroy the singular behavior of the rate function r_a. The vortex excitation in 2D Kitaev model is adiabatic with temperature and does not induce any phase transition [64]. Hence the vortex-free configuration gives the main contribution to the nonanalytic feature of the rate function at nonzero temperatures.

VI. THREE-DIMENSIONAL CASE

In the case of applying our detector to 3D Hamiltonians, we consider two types of topological materials, namely, the Weyl semimetals and the topological nodal line semimetal.

A. Weyl semimetal

The commuting Hamiltonians for Weyl semimetals can be written as [65,66],

$$\mathcal{H}_{\vec{q}} = a_{\vec{q}}\sigma_1 + b_{\vec{q}}\sigma_2 + c_{\vec{q}}\sigma_3 \tag{37}$$

where $a_{\vec{q}} = \sin(q_x)$, $b_{\vec{q}} = \sin(q_y)$, $c_{\vec{q}} = J_3 - \cos(q_x) - \cos(q_y) - \cos(q_z)$ and $\vec{q}$ runs over a simple cubic lattice in the range $(-\pi < q_x, q_y, q_z < \pi)$.

The ground state of this Hamiltonian shows a gapless phase for $J_3 < 3$ and a gapped phase for $J_3 > 3$. We consider a quench $J_3 = J_0 \to J_3 = J$.

We numerically evaluate the rate function r_a from Eq. (9),

$$r_a(\beta, J_0, J) = 3\log 2 - \frac{1}{8\pi^3}\int_{\vec{q}} \log(1 + \alpha_{\vec{q}})d\vec{q} - \frac{1}{4\pi^3}\int_{\vec{q}} \log[1 + \sqrt{1 - \gamma_{\vec{q}}\mathcal{L}_{\vec{q}}}]d\vec{q} \tag{38}$$

where $p = J$, $V = 8\pi^3$ and $\mathcal{L}_{\vec{q}}$ for Weyl semimetal is

$$\mathcal{L}_{\vec{q}} = (J - J_0)^2(\sin^2(q_x) + \sin^2(q_y))/(\lambda_{\vec{q}}\lambda'_{\vec{q}})^2. \tag{39}$$

We observe that the first derivative (with respect to J) of r_a shows a change of slope at the QCP $J = 3$ both for $J_0 < 3$ and >3 (Fig. 7) and the double derivative diverges algebraically with a critical exponent $1/3$ (Fig. 8). It is important to mention that, unlike the previous two cases, this singularity is visible only at low temperatures and we could not study the behavior of r_a analytically.

B. Topological nodal line semimetal

When $b_{\vec{q}} = 0$ in Eq. (37), one has a topological nodal line semimetal [67]. We write the commuting Hamiltonians as

$$\mathcal{H}_{\vec{q}} = a_{\vec{q}}\sigma_1 + c_{\vec{q}}\sigma_3 \tag{40}$$

where $c_{\vec{q}} = J_3 - \cos(q_x) - \cos(q_y) - \cos(q_z)$ and $a_{\vec{q}} = \sin(q_z)$. Usually one uses the Hamiltonian

$$\mathcal{H}^0_{\vec{k}} = vk_z\sigma_x + \left(k^2 - k_0^2\right)\sigma_z \tag{41}$$

(with v and k_0 as parameters) for this type of materials [65,68,69]. The Hamiltonian of Eq. (40) reduces to this form on the plane $k_x = -k_y$, up to terms quadratic in $\vec{k}$.

The Hamiltonian (40) has a gapped phase in the region $J_3 > 3$ while it shows a gapless phase when $J_3 < 3$. For a quench $J_3 = J_0$ to $J_3 = J$, the rate function r_a is calculated from Eq. (38) with

$$\mathcal{L}_{\vec{q}} = (J - J_0)^2(\sin(q_z))^2/(\lambda_{\vec{q}}\lambda'_{\vec{q}})^2. \tag{42}$$

In this case also, one observes a change of slope at $J = 3$ of the curve $\partial r_a/\partial J$ vs J (Fig. 9). The second derivative does not show any divergence at the critical point but has a finite discontinuity (Fig. 10). It is important to mention that the discontinuity becomes smaller as temperature increases and we could not study the behavior of r_a analytically in this case.

C. A topological insulator Bi_4Br_4

Single-layer Bi_4Br_4 is a quantum spin Hall insulating material. It has been shown that topological edge states persist in

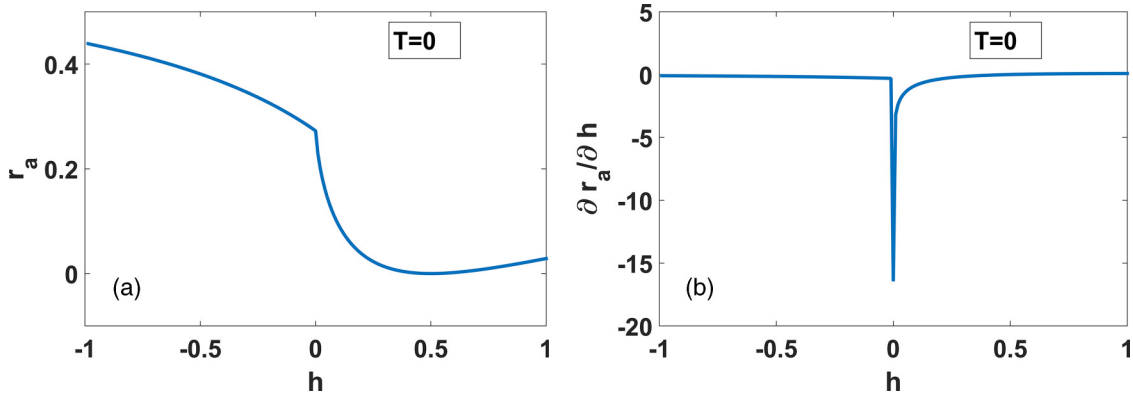

FIG. 13. Rate function r_a (a) and its derivative (b) for 1D XY Model computed from Eq. (46) at zero temperature with the prequench parameter $h_0 = 0.5$. Nonanalyticity appears only at the phase boundary $h = 0$.

multilayer Bi_4Br_4 even at room temperature [49,50] and that it is a suitable candidate for a room-temperature topological insulator for its large band gap [49,70–74]. A low-energy effective $k \cdot p$ Hamiltonian for a single layer has been suggested for this material [49], and in this section we shall show that our rate function computed using this Hamiltonian correctly predicts the phase transition.

The suggested Hamiltonian is

$$\mathcal{H} = \begin{bmatrix} M & A_1 q_x & 0 & A_2 q_y \\ A_1^* q_x & -M & A_2 q_y & 0 \\ 0 & A_2^* q_y & M & -A_1^* q_x \\ A_2^* q_y & 0 & -A_1 q_x & -M \end{bmatrix} \tag{43}$$

where

$$M = M_0 - B_1 q_x^2 - B_2 q_y^2 \tag{44}$$

and $A_1 = -1.81 + i0.0461$ eV Å, $A_2 = -4.15 + i0.141$ eV Å, $B_1 = 3.86$ eV Å^2, $B_2 = 0.0032$ eV Å^2. We will quench the parameter M_0 from M_0 to M_0' as the quantum critical point is at $M_0 = 0$ eV. Using the fact that the square of this Hamiltonian is a scalar times unit matrix, one can calculate the exponentials for prequench and postquench Hamiltonian, and carry on the calculation of rate function following Sec. II. The result is an equation similar to Eq. (38),

$$r_a(\beta, J_0, J) = 4\log 2 - \frac{1}{V}\int_{\vec{q}} \log(1+\alpha_{\vec{q}})d\vec{q} - \frac{2}{V}\int_{\vec{q}} \log[1+\sqrt{1-\gamma_{\vec{q}}\mathcal{L}_{\vec{q}}}]d\vec{q} \tag{45}$$

with

$$\mathcal{L}_{\vec{q}} = \frac{1}{2} - \frac{X}{2\lambda^2\lambda'^2}$$
$$X = \left(MM' + |A_1|^2 q_x^2 + |A_2|^2 q_y^2\right)^2 - |A_1|^2 q_x^2 (M'-M)^2 - |A_2|^2 q_y^2 (M'-M)^2$$
$$M' = M_0' - B_1 q_x^2 - B_2 q_y^2$$

where V is the area of the region of integration close to origin (see Fig. 11). The numerically computed rate function and its derivative as obtained from Eq. (45) are plotted against the postquench value M_0' in Fig. 11. It shows a divergence in its second derivative at $M_0' = 0$ at room temperature. Divergence in second derivative can also be obtained at other temperatures. This shows that our procedure works for the material Bi_4Br_4, in spite of the fact that the Hamiltonian is made up of 4×4 commuting matrices instead of 2×2 ones [see Eqs. (5) and (43)].

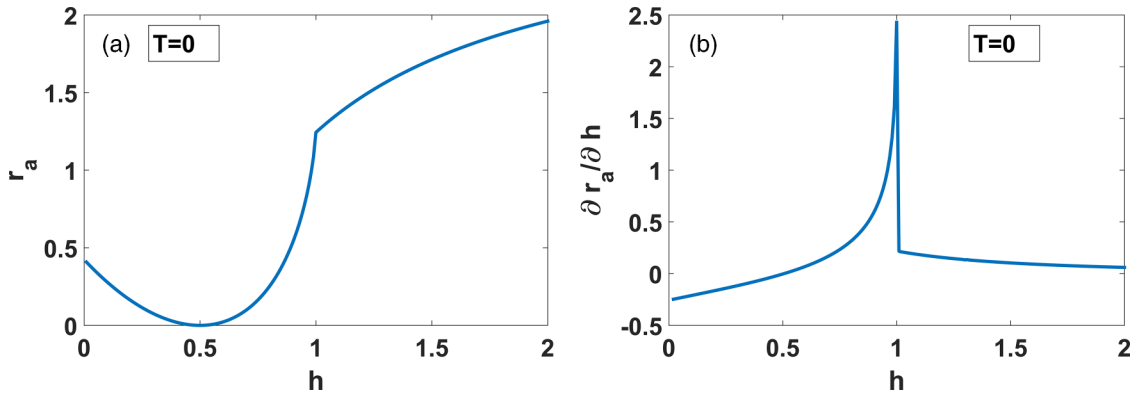

FIG. 14. Rate function r_a (a) and its derivative (b) for 1D SSH Model computed from Eq. (46) at zero temperature with the prequench parameter $h_0 = 0.5$. Nonanalyticity appears only at the phase boundary $h = 1$.

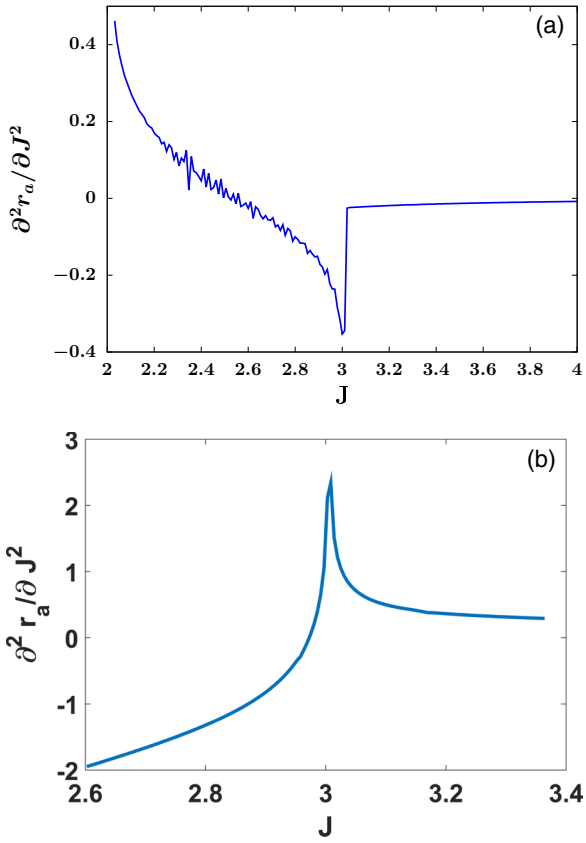

FIG. 15. Rate function r_a and its derivative for (a) 3D topological nodal line semimetal and (b) Weyl semimetal computed from Eq. (46) at zero temperature with $J_0 = 2$ for TNLSM and $J_0 = 2.5$ for Weyl semimetal. Nonanalyticity appears only at the phase boundary $J = 3$. The oscillations in plot (a) is due to computational constraint.

VII. ZERO-TEMPERATURE BEHAVIOR

At zero temperature, the rate function in Eq. (3) reduces to the rate function used to define dynamical quantum phase transition [37] using Loschmidt echo. The system undergoing dynamical phase transition shows nonanalytic peaks when rate function is plotted against time. The seminal idea was that a system undergoes dynamical quantum phase transition only if the system is quenched across the equilibrium quantum critical point. Transverse Ising model shows such behavior. But later it has been shown that there may not be nonanalyticity in the rate function versus time plot when the quench is across the critical point or there may be a nonanalyticity when the quench is not across the critical point [48,62,75]. We show here that the long-time limit of our rate function at $T = 0$ shows nonanalyticity only if the system is quenched across the critical point. Our observation holds for all the Hamiltonians considered in this paper. The long-time limit of the rate function (9) at zero temperature will become

$$r_a = 2\log 2 - \frac{2}{V}\int_{\vec{q}} \log[1+\sqrt{1-\mathcal{L}_{\vec{q}}}]d\vec{q}. \tag{46}$$

We have plotted this function and its derivative for different cases in Figs. 12–15. The plots shows nonanalyticity only at the the quantum critical point.

VIII. CONCLUSIONS

We explore the response of the fidelity at finite temperature in topological systems, which can be mapped to free fermionic Hamiltonians and observe a nonanalyticity at the corresponding phase boundaries in different dimensions. The rate function in this case can be written as a series, each term of which has an integral independent of temperature, while the prefactors of the integrals contain temperature. We could show that the integral brings about the nonanalytic behavior and hence the signature persists at high temperature also.

In case of 1D and 2D Hamiltonians, the reason behind the nonanalytic behavior of the quantity could be explained by mapping the integral to the complex plane and identifying a change of pole structure at the quantum critical point. The amount of the discontinuity or the exponent of the divergence as the case may be, could also be determined. However, analytical explanation was not possible in the case of 3D Hamiltonians. We suspect that the numerical limitation is the reason behind the signature being visible at low temperatures only. More investigation in this direction is in progress.

We have also shown that the long-time limit of the rate function r_a shows nonanalyticity only at QCP at $T = 0$ while the nonanalyticity in rate function for Loschmidt echo versus time plots may not correspond with a quench across QCP.

A question that immediately comes to mind is whether this signature has the robustness beyond three dimension. Our primary conjecture is that it has the robustness because the concerned integral would just turn into a d-dimensional one. However, more detailed studies are needed to confirm this. It would also be interesting to explore how our rate function behaves for other integrable and nonintegrable Hamiltonians.

ACKNOWLEDGMENTS

The authors acknowledge anonymous referees for constructive opinions on an early version of this paper. P.N. acknowledges University Grants Commission, India for financial support (Ref. No. 191620072523) and Harish Chandra Research Institute for access to their infrastructure.

APPENDIX A

In this Appendix we present the detailed derivation for the expressions of rate function in Eqs. (8), (9), and (10). From the expressions for $\mathcal{H}_{\vec{q}}$ and $\mathcal{H}'_{\vec{q}}$ in Eq. (6) and the equation next to it, we can write the matrix product of $(\hat{\mathcal{V}}_{\vec{q}}\cdot\vec{\sigma})$ and $(\hat{\mathcal{V}}'_{\vec{q}}\cdot\vec{\sigma})$ as

$$(\hat{\mathcal{V}}_{\vec{q}}\cdot\vec{\sigma})(\hat{\mathcal{V}}'_{\vec{q}}\cdot\vec{\sigma}) = \vec{\mathcal{V}}\cdot\vec{\mathcal{V}}'\,\underline{1} + i[\vec{\mathcal{V}}\times\vec{\mathcal{V}}']\cdot\vec{\sigma}.$$

Since

$$\mathcal{H}_{\vec{q}}^2 = \lambda_{\vec{q}}^2\underline{1} \quad \text{and} \quad \mathcal{H}_{\vec{q}}'^{\,2} = \lambda_{\vec{q}}'^{\,2}\underline{1}$$

we get

$$\begin{aligned} e^{-\beta\mathcal{H}_{\vec{q}}}\cdot e^{-it\mathcal{H}'_{\vec{q}}} &= [\cosh(\beta\lambda)\cos(\lambda' t) + i\sinh(\beta\lambda)\sin(\lambda' t)\,\vec{\mathcal{V}}\cdot\vec{\mathcal{V}}']\underline{1} \\ &\quad - \vec{\sigma}\cdot[\sinh(\beta\lambda)\cos(\lambda' t)\,\vec{\mathcal{V}} + i\cosh(\beta\lambda)\sin(\lambda' t)\,\vec{\mathcal{V}}' \\ &\quad + \sinh(\beta\lambda)\sin(\lambda' t)\,\vec{\mathcal{V}}\times\vec{\mathcal{V}}']. \end{aligned} \tag{A1}$$

By reversing the sign of t in this expression, one can obtain the expression for $\rho_0 e^{it\mathcal{H}'}$. One can now calculate $\rho_0\rho_t = \rho_0 e^{-it\mathcal{H}'}\rho_0 e^{it\mathcal{H}'}$ and take the trace of it. The result is

$$\frac{\mathrm{Tr}(\rho_0\rho_t)}{[\mathrm{Tr}(\rho_0)]^2} = \frac{1}{2}[1+\tanh^2(\beta\lambda) - 2\mathcal{L}\,\tanh^2(\beta\lambda)\sin^2(\lambda' t)] \tag{A2}$$

where

$$\mathcal{L} = \tfrac{1}{2}[1+|\vec{\mathcal{V}}\times\vec{\mathcal{V}}'|^2 - (\vec{\mathcal{V}}\cdot\vec{\mathcal{V}}')^2]. \tag{A3}$$

Since $\vec{\mathcal{V}}$ and $\vec{\mathcal{V}}'$ are unit vectors,

$$\mathcal{L} = 1 - |\vec{\mathcal{V}}\cdot\vec{\mathcal{V}}'|^2 = \sin^2(\phi) \tag{A4}$$

where ϕ is the angle between the vectors $\vec{\mathcal{V}}$ and $\vec{\mathcal{V}}'$.

Using standard results [52], we get the long-time limit as

$$r_a(\beta, p_0, p) = 3\log 2 - \frac{1}{V}\int_{\vec{q}}\log(1+\alpha_{\vec{q}})d\vec{q} - \frac{2}{V}\int_{\vec{q}}\log[1+\sqrt{1-\gamma_{\vec{q}}\mathcal{L}_{\vec{q}}}]d\vec{q} \tag{A5}$$

with $\alpha_{\vec{q}} = \tanh^2(\beta\lambda_{\vec{q}})$, $\gamma_{\vec{q}} = 2\alpha_{\vec{q}}/(1+\alpha_{\vec{q}}) = 1-\mathrm{sech}(2\beta\lambda_{\vec{q}})$ and $V = \int_{\vec{q}} d\vec{q}$. We now note that $0 < \gamma_{\vec{q}}\mathcal{L}_{\vec{q}} < 1$ and use the expansion

$$\log[1+\sqrt{1-x}] = \log 2 + \tfrac{1}{4}\left(x + \tfrac{3}{8}x^2 + \tfrac{5}{24}x^3\cdots\right) \tag{A6}$$

to arrive at Eq. (10).

APPENDIX B

In this Appendix, we consider Kitaev model on honeycomb lattice and show analytically that the double derivative diverges at the critical point with an exponent $1/2$ at all temperatures. We consider the quench of J_3 from J_0 to J at time $t = 0$.

We shall start by calculating I_1, which we obtain by putting $n = 1$ in Eq. (33),

$$I_1 = 4(J-J_0)^2\int_{u=0}^{\pi/2} du \int_{v=-\pi}^{\pi} dv \left(\frac{a'}{\lambda'}\right)^2 \tag{B1}$$

where the primed quantities are the value of b and λ after quench. We have dropped the subscript $\vec{q}$ for brevity.

By substituting $z = e^{iv}$, we can write I_1 as

$$I_1 = -\frac{i(J-J_0)^2}{J}\int_0^{\frac{\pi}{2}} du \oint_{\mathcal{C}} dz F(z) \tag{B2}$$

where $\mathcal{C}$ is the unit circle and

$$F(z) = \frac{z_0\left(z^2 - \frac{\bar{z}_0}{z_0}\right)^2}{z^2\left(z-\frac{J}{z_0}\right)\left(z-\frac{\bar{z}_0}{J}\right)} \tag{B3}$$

with $z_0 = M\cos(u) + iN\sin(u)$.

The poles of $F(z)$ are $z_1 = 0$, $z_2 = J/z_0$ and $z_3 = \bar{z}_0/J$ and the respective residues are

$$R_1 = \frac{\bar{z}_0}{J} + \frac{J}{z_0},$$
$$R_2 = -\frac{\bar{z}_0}{J} + \frac{J}{z_0},$$
$$R_3 = \frac{\bar{z}_0}{J} - \frac{J}{z_0}. \tag{B4}$$

The poles z_1 and z_2 are inside the unit circle when $u < u_c$ and z_1 and z_3 are inside the unit circle when $u > u_c$ where u_c follows the relation

$$\cos(u_c) = \sqrt{\frac{(J+N)(J-N)}{4J_1J_2}}.$$

By applying the residue theorem, we can evaluate the integral I_1 as

$$I_1 = \frac{2\pi}{J}(J-J_0)^2\left[2Ju_c - (M^2-N^2)\frac{\sin(2u_c)}{2J} + \frac{1}{J}(M^2+N^2)\left(\frac{\pi}{2}-u_c\right)\right]. \tag{B5}$$

When J approaches M from below, we can replace J by $M-\epsilon$ in Eq. (B.5) where ϵ is very small and differentiating I_1 with respect to J we get

$$\frac{\partial^2 I_1}{\partial J^2} \approx -\frac{4\pi\sqrt{2}(M-J_0)^2}{(M(M^2-N^2))^{\frac{1}{2}}}\epsilon^{-\frac{1}{2}} \tag{B6}$$

up to leading order.

When J approaches $|N|$ from below, we can replace J by $|N|+\epsilon$ in Eq. (B.5) where ϵ is small and differentiating I_1 with respect to J we get

$$\frac{\partial^2 I_1}{\partial J^2} \approx -\frac{4\pi\sqrt{2}(|N|-J_0)^2}{(|N|(M^2-N^2))^{\frac{1}{2}}}\epsilon^{-\frac{1}{2}} \tag{B7}$$

up to leading order.

This proves that at high temperature where I_1 is the dominant term, the double derivative of the rate function will diverge with an exponent $1/2$ at both the critical points. But at lower temperature, I_n with $n > 1$ will also contribute to the double derivative. We will show that the critical exponent will be unchanged for I_n with $n > 1$. We need to calculate the integral I_n, which after substitution $z = e^{iv}$ can be written as

$$I_n = -\frac{4i(J-J_0)^{2n}}{(4J)^n}\int_0^{\frac{\pi}{2}} du \oint F^{(n)} dz \tag{B8}$$

where

$$F^{(n)} = \frac{z_0^n\left(z^2-\frac{\bar{z}_0}{z_0}\right)^{2n}}{z^{n+1}\left(z-\frac{J}{z_0}\right)^n\left(z-\frac{\bar{z}_0}{J}\right)^n}. \tag{B9}$$

By applying residue theorem, we can write the integral I_n as

$$I_n = \frac{8\pi(J-J_0)^{2n}}{(4J)^n}\left[\int_0^{\frac{\pi}{2}} R_1^{(n)}du + \int_0^{u_c} R_2^{(n)}du + \int_{u_c}^{\frac{\pi}{2}} R_3^{(n)}du\right]$$

where $R_1^{(n)}$, $R_2^{(n)}$, and $R_3^{(n)}$ are the residues of the poles $z_1 = 0$, $z_2 = J/z_0$, and $z_3 = \bar{z}_0/J$ respectively.

Since the nonanalyticity arises from the residues $R_2^{(n)}$ and $R_3^{(n)}$, we will prove that both $R_2^{(n)}$ and $R_3^{(n)}$ are proportional to R_2 and R_3 respectively up to leading order.

We can write R_2^n as

$$R_2^{(n)} = \lim_{z\to z_2}\frac{1}{(n-1)!}\frac{d^{n-1}}{dz^{n-1}}\frac{z_0^n\left(z^2-\frac{\bar{z}_0}{z_0}\right)^{2n}}{z^{n+1}\left(z-\frac{\bar{z}_0}{J}\right)^n} = \lim_{z\to z_2}\frac{1}{(n-1)!}\frac{d^{n-1}}{dz^{n-1}}\frac{G^n}{z} \tag{B10}$$

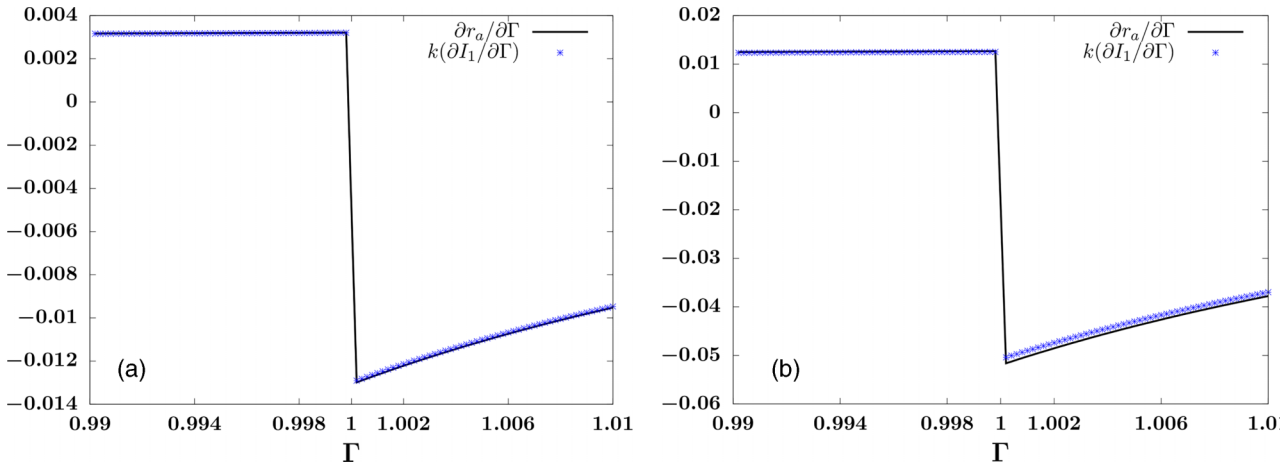

FIG. 16. Transverse XY model. The plot shows that discontinuity in $\partial r_a/\partial\Gamma$ comes mainly from the discontinuity in $\partial I_1/\partial\Gamma$ at high temperatures. k is the constant $(c_1\gamma)/(2V\lambda^2)$, which is multiplied to I_1 in Eq. (11). Panel (a) is for $\beta = 0.1$ and panel (b) is for $\beta = 0.2$. Both the cases are for quench of Γ parameter.

where we define $G(z)$ as

$$G(z) = \frac{z_0\left(z^2 - \frac{\bar{z}_0}{z_0}\right)^2}{z\left(z - \frac{\bar{z}_0}{J}\right)}. \tag{B11}$$

We observe that

$$\frac{d^{n-1}(G^n/z)}{dz^{n-1}} = \frac{G}{z}\left[n!\left(\frac{dG}{dz}\right)^{n-1} + \Gamma\right] \tag{B12}$$

where Γ contains the terms, which will involve G^k or G^k/z as a factor where $k \geqslant 1$. We know that $(G/z)_{z=z_2} = R_2^1$ and $(dG/dz)_{z=z_2} = 2J + z_0\bar{z}_0/J$. Therefore

$$\left(\frac{dG}{dz}|_{z=z_2}\right)^{n-1} \approx \left(\frac{2M^2 + z_0\bar{z}_0}{M}\right)^{n-1}(1 + c\epsilon)^{n-1}$$
$$\text{when } J = M - \epsilon,$$
$$\left(\frac{dG}{dz}|_{z=z_2}\right)^{n-1} \approx \left(\frac{2N^2 + z_0\bar{z}_0}{|N|}\right)^{n-1}(1 + c'\epsilon)^{n-1}$$
$$\text{when } J = |N| + \epsilon,$$

where c and c' are constants. Putting the values of $(\frac{dG}{dz}|_{z=z_2})^{n-1}$ and $(\frac{G}{z})_{z=z_2}$, we get

$$R_2^{(n)} \approx n\left(\frac{2M^2 + z_0\bar{z}_0}{M}\right)^{n-1} R_2^{(1)} \quad \text{when } J = M - \epsilon,$$

$$R_2^{(n)} \approx n\left(\frac{2N^2 + z_0\bar{z}_0}{|N|}\right)^{n-1} R_2^{(1)} \quad \text{when } J = |N| + \epsilon. \tag{B13}$$

Similar calculation can be done for $R_3^{(n)}$. Thus we prove that I_n will also diverge with an exponent $1/2$ at both quantum critical points.

APPENDIX C

In the Figs. 16–18 we show numerically that the discontinuity in the single derivative of the rate function with respect to the final value of the quench parameter can be approximated by the derivative of the $n = 1$ term in Eq (11) for the

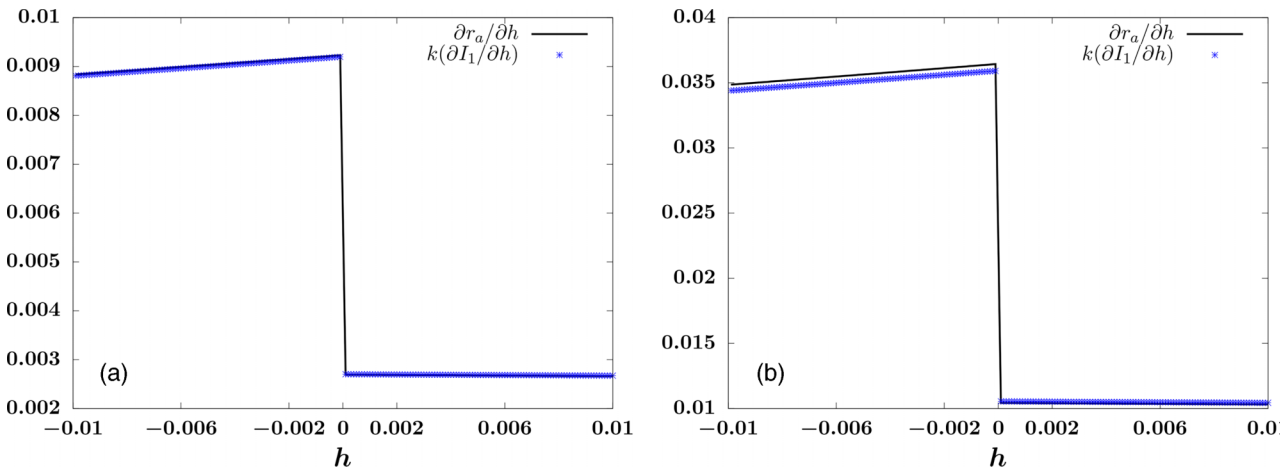

FIG. 17. Transverse XY model. The plot shows that discontinuity in $\partial r_a/\partial h$ comes mainly from the discontinuity in $\partial I_1/\partial h$ at high temperatures. k is the constant $(c_1\gamma)/(2V\lambda^2)$, which is multiplied to I_1 in Eq (11). Panel (a) is for $\beta = 0.1$ and panel (b) is for $\beta = 0.2$. Both the cases are for quench of h parameter.

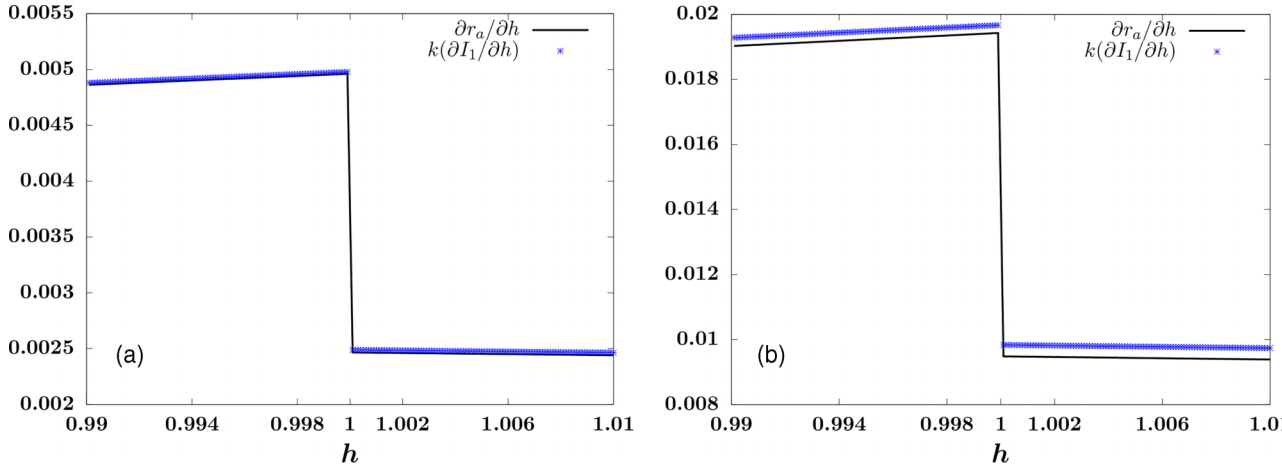

FIG. 18. SSH model. The plot shows that discontinuity in $\partial r_a/\partial h$ comes mainly from the discontinuity in $\partial I_1/\partial h$ at high temperatures. k is the constant $(c_1\gamma)/(2V\lambda^2)$, which is multiplied to I_1 in Eq. (11). Panel (a) is for $\beta = 0.1$ and panel (b) is for $\beta = 0.2$. Both the cases are for quench of h parameter.

one-dimensional models at high temperatures. The fact that near-critical point behavior of the rate function can be approximated by I_1 even for 2D Kitaev model at high temperatures was established in [36].

[1] S. Sachdev, *Quantum Phase Transitions*, 2nd ed. (Cambridge University Press, Cambridge, 2011)

[2] S. Hofferberth, I. Lesanovsky, T. Schumm, A. Imambekov, V. Gritsev, E. Demler, and J. Schmiedmayer, Probing quantum and thermal noise in an interacting many-body system, Nat. Phys. **4**, 489 (2008).

[3] M. Campisi, P. Hänggi, and P. Talkner, Colloquium: Quantum fluctuation relations: Foundations and applications, Rev. Mod. Phys. **83**, 771 (2011).

[4] M. Greiner, O. Mandel, T. Esslinger, T. W. Hänsch, and I. Bloch, Quantum phase transition from a superfluid to a Mott insulator in a gas of ultracold atoms, Nature (London) **415**, 39 (2002).

[5] E. Haller, R. Hart, M. J. Mark, J. G. Danzl, L. Reichsöllner, M. Gustavsson, M. Dalmonte, G. Pupillo, and H.-C. Nägerl, Pinning quantum phase transition for a Luttinger liquid of strongly interacting bosons, Nature (London) **466**, 597 (2010).

[6] X. Zhang, C.-L. Hung, S.-K. Tung, and C. Chin, Observation of quantum criticality with ultracold atoms in optical lattices, Science **335**, 1070 (2012).

[7] X.-W. Guan, M. T. Batchelor, and C. Lee, Fermi gases in one dimension: From Bethe ansatz to experiments, Rev. Mod. Phys. **85**, 1633 (2013).

[8] S. L. Sondhi, S. M. Girvin, J. P. Carini, and D. Shahar, Continuous quantum phase transitions, Rev. Mod. Phys. **69**, 315 (1997).

[9] P. Zanardi and N. Paunković, Ground state overlap and quantum phase transitions, Phys. Rev. E **74**, 031123 (2006).

[10] P. Zanardi, M. Cozzini, and P. Giorda, Ground state fidelity and quantum phase transitions in free Fermi systems, J. Stat. Mech. (2007) L02002.

[11] M. Cozzini, P. Giorda, and P. Zanardi, Quantum phase transitions and quantum fidelity in free fermion graphs, Phys. Rev. B **75**, 014439 (2007).

[12] H.-Q. Zhou and J. P. Barjaktarevic, Fidelity and quantum phase transitions, J. Phys. A: Math. Theor. **41**, 412001 (2008).

[13] S.-J. Gu, Fidelity approach to quantum phase transitions, Int. J. Mod. Phys. B **24**, 4371 (2010).

[14] B. Damski, Fidelity approach to quantum phase transitions in quantum Ising model, in *Quantum Criticality in Condensed Matter: Phenomena, Materials and Ideas in Theory and Experiment* (World Scientific, Singapore, 2016), pp. 159–182.

[15] N. T. Jacobson, L. C. Venuti, and P. Zanardi, Unitary equilibration after a quantum quench of a thermal state, Phys. Rev. A **84**, 022115 (2011).

[16] P. Zanardi, H. T. Quan, X. Wang, and C. P. Sun, Mixed-state fidelity and quantum criticality at finite temperature, Phys. Rev. A **75**, 032109 (2007).

[17] S. T. Amin, B. Mera, C. Vlachou, N. Paunković, and V. R. Vieira, Fidelity and Uhlmann connection analysis of topological phase transitions in two dimensions, Phys. Rev. B **98**, 245141 (2018).

[18] H. T. Quan and F. M. Cucchietti, Quantum fidelity and thermal phase transitions, Phys. Rev. E **79**, 031101 (2009).

[19] Y.-W. Dai, Q.-Q. Shi, S. Y. Cho, M. T. Batchelor, and H.-Q. Zhou, Finite-temperature fidelity and von neumann entropy in the honeycomb spin lattice with quantum Ising interaction, Phys. Rev. B **95**, 214409 (2017).

[20] Y.-C. Liang, Y.-H. Yeh, P. E. M. F. Mendonça, R. Y. Teh, M. D. Reid, and P. D. Drummond, Quantum fidelity measures for mixed states, Rep. Prog. Phys. **82**, 076001 (2019).

[21] M. Białończyk, F. J. Gómez-Ruiz, and A. del Campo, Uhlmann fidelity and fidelity susceptibility for integrable spin chains at finite temperature: exact results, New J. Phys. **23**, 093033 (2021).

[22] B. Mera, C. Vlachou, N. Paunković, V. R. Vieira, and O. Viyuela, Dynamical phase transitions at finite temperature from fidelity and interferometric Loschmidt echo induced metrics, Phys. Rev. B **97**, 094110 (2018).

[23] Y. C. Li, J. Zhang, and H.-Q. Lin, Quantum coherence spectrum and quantum phase transitions, Phys. Rev. B **101**, 115142 (2020).

[24] S. Haldar, S. Roy, T. Chanda, and A. Sen(De), Response of macroscopic and microscopic dynamical quantifiers to the quantum critical region, Phys. Rev. Res. **2**, 033249 (2020).

[25] S. Roy, R. Moessner, and A. Das, Locating topological phase transitions using nonequilibrium signatures in local bulk observables, Phys. Rev. B **95**, 041105(R) (2017).

[26] X.-Y. Hou, Q.-C. Gao, H. Guo, and C.-C. Chien, Metamorphic dynamical quantum phase transition in double-quench processes at finite temperatures, Phys. Rev. B **106**, 014301 (2022).

[27] N. O. Abeling and S. Kehrein, Quantum quench dynamics in the transverse field Ising model at nonzero temperatures, Phys. Rev. B **93**, 104302 (2016).

[28] A. A. Zvyagin, Staggered field induced dynamical effects in a quantum spin chain, Phys. Rev. B **97**, 214425 (2018).

[29] A. A. Zvyagin, Pulse dynamics of quantum systems with pairing, Phys. Rev. B **92**, 184507 (2015).

[30] A. A. Zvyagin, Nonequilibrium dynamics of a system with two kinds of fermions after a pulse, Phys. Rev. B **95**, 075122 (2017).

[31] A. A. Zvyagin, Dynamical quantum phase transitions (Review Article), Low Temp. Phys. **42**, 971 (2016).

[32] A. Zvyagin, *Quantum Theory of One-Dimensional Spin Systems*, Kharkov Series in Physics and Mathematics (Cambridge University Press, Cambridge, 2010).

[33] S. Bandyopadhyay, A. Polkovnikov, and A. Dutta, Late-time critical behavior of local stringlike observables under quantum quenches, Phys. Rev. B **107**, 064105 (2023).

[34] G. A. P. Ribeiro and G. Rigolin, Detecting quantum critical points at finite temperature via quantum teleportation, Phys. Rev. A **107**, 052420 (2023).

[35] G. Ribeiro and G. Rigolin, Detecting quantum critical points at finite temperature via quantum teleportation: Further models, Phys. Rev. A **109**, 012612 (2024).

[36] P. Nandi, S. Bhattacharyya, and S. Dasgupta, Detection of quantum phase boundary at finite temperatures in integrable spin models, Phys. Rev. Lett. **128**, 247201 (2022).

[37] M. Heyl, A. Polkovnikov, and S. Kehrein, Dynamical quantum phase transitions in the transverse-field Ising model, Phys. Rev. Lett. **110**, 135704 (2013).

[38] C. Karrasch and D. Schuricht, Dynamical phase transitions after quenches in nonintegrable models, Phys. Rev. B **87**, 195104 (2013).

[39] J. N. Kriel, C. Karrasch, and S. Kehrein, Dynamical quantum phase transitions in the axial next-nearest-neighbor Ising chain, Phys. Rev. B **90**, 125106 (2014).

[40] E. Canovi, P. Werner, and M. Eckstein, First-order dynamical phase transitions, Phys. Rev. Lett. **113**, 265702 (2014).

[41] M. Heyl, Dynamical quantum phase transitions in systems with broken-symmetry phases, Phys. Rev. Lett. **113**, 205701 (2014).

[42] J. M. Hickey, S. Genway, and J. P. Garrahan, Dynamical phase transitions, time-integrated observables, and geometry of states, Phys. Rev. B **89**, 054301 (2014).

[43] F. Andraschko and J. Sirker, Dynamical quantum phase transitions and the Loschmidt echo: A transfer matrix approach, Phys. Rev. B **89**, 125120 (2014).

[44] A. J. A. James and R. M. Konik, Quantum quenches in two spatial dimensions using chain array matrix product states, Phys. Rev. B **92**, 161111(R) (2015).

[45] S. Vajna and B. Dóra, Topological classification of dynamical phase transitions, Phys. Rev. B **91**, 155127 (2015).

[46] M. Heyl, Scaling and universality at dynamical quantum phase transitions, Phys. Rev. Lett. **115**, 140602 (2015).

[47] J. C. Budich and M. Heyl, Dynamical topological order parameters far from equilibrium, Phys. Rev. B **93**, 085416 (2016).

[48] S. Vajna and B. Dóra, Disentangling dynamical phase transitions from equilibrium phase transitions, Phys. Rev. B **89**, 161105(R) (2014).

[49] J.-J. Zhou, W. Feng, G.-B. Liu, and Y. Yao, Topological edge states in single- and multi-layer Bi_4Br_4, New J. Phys. **17**, 015004 (2015).

[50] N. Shumiya, M. S. Hossain, J.-X. Yin, Z. Wang, M. Litskevich, C. Yoon, Y. Li, Y. Yang, Y.-X. Jiang, G. Cheng *et al.*, Evidence of a room-temperature quantum spin Hall edge state in a higher-order topological insulator, Nat. Mater. **21**, 1111 (2022).

[51] M. Heyl, Dynamical quantum phase transitions: A review, Rep. Prog. Phys. **81**, 054001 (2018).

[52] I. S. Gradshteyn and I. M. Ryzhik, *Table of Integrals, Series, and Products* (Academic Press, New York, 2014).

[53] E. Lieb, T. Schultz, and D. Mattis, Two soluble models of an antiferromagnetic chain, Ann. Phys. **16**, 407 (1961).

[54] P. Pfeuty, The one-dimensional Ising model with a transverse field, Ann. Phys. **57**, 79 (1970).

[55] W. P. Su, J. R. Schrieffer, and A. J. Heeger, Solitons in polyacetylene, Phys. Rev. Lett. **42**, 1698 (1979).

[56] W. P. Su, J. R. Schrieffer, and A. J. Heeger, Soliton excitations in polyacetylene, Phys. Rev. B **22**, 2099 (1980).

[57] A. Kitaev, Anyons in an exactly solved model and beyond, Ann. Phys. **321**, 2 (2006).

[58] X.-Y. Feng, G.-M. Zhang, and T. Xiang, Topological characterization of quantum phase transitions in a spin-1/2 model, Phys. Rev. Lett. **98**, 087204 (2007).

[59] A. Kitaev and C. Laumann, *Topological Phases and Quantum Computation* (Oxford University Press, Oxford, 2010), p. 101.

[60] K. Sengupta, D. Sen, and S. Mondal, Exact results for quench dynamics and defect production in a two-dimensional model, Phys. Rev. Lett. **100**, 077204 (2008).

[61] S. Mondal, D. Sen, and K. Sengupta, Quench dynamics and defect production in the Kitaev and extended Kitaev models, Phys. Rev. B **78**, 045101 (2008).

[62] M. Schmitt and S. Kehrein, Dynamical quantum phase transitions in the Kitaev honeycomb model, Phys. Rev. B **92**, 075114 (2015).

[63] U. Bhattacharya, S. Dasgupta, and A. Dutta, Dynamical merging of Dirac points in the periodically driven Kitaev honeycomb model, Eur. Phys. J. B **89**, 1 (2016).

[64] J. Nasu, M. Udagawa, and Y. Motome, Vaporization of Kitaev spin liquids, Phys. Rev. Lett. **113**, 197205 (2014).

[65] N. P. Armitage, E. J. Mele, and A. Vishwanath, Weyl and Dirac semimetals in three-dimensional solids, Rev. Mod. Phys. **90**, 015001 (2018).

[66] S. Rao, Weyl semi-metals: A short review, arXiv:1603.02821.

[67] R. Okugawa and S. Murakami, Universal phase transition and band structures for spinless nodal-line and Weyl semimetals, Phys. Rev. B **96**, 115201 (2017).

[68] A. A. Burkov, M. D. Hook, and L. Balents, Topological nodal semimetals, Phys. Rev. B **84**, 235126 (2011).

[69] M. Yang, W. Luo, and W. Chen, Quantum transport in topological nodal-line semimetals, Adv. Phys.: X **7**, 2065216 (2022).

[70] J.-J. Zhou, W. Feng, C.-C. Liu, S. Guan, and Y. Yao, Large-gap quantum spin hall insulator in single layer bismuth monobromide Bi_4Br_4, Nano Lett. **14**, 4767 (2014).

[71] C.-C. Liu, J.-J. Zhou, Y. Yao, and F. Zhang, Weak topological insulators and composite Weyl semimetals: β-Bi_4X_4 (X = Br, I), Phys. Rev. Lett. **116**, 066801 (2016).

[72] C.-H. Hsu, X. Zhou, Q. Ma, N. Gedik, A. Bansil, V. M. Pereira, H. Lin, L. Fu, S.-Y. Xu, and T.-R. Chang, Purely rotational symmetry-protected topological crystalline insulator α-Bi_4Br_4, 2D Mater. **6**, 031004 (2019).

[73] X. Li, D. Chen, M. Jin, D. Ma, and E. A. Yanfeng Ge, Pressure-induced phase transitions and superconductivity in a quasi-1-dimensional topological crystalline insulator α-Bi_4Br_4, Proc. Natl. Acad. Sci. USA **116**, 17696 (2019).

[74] C. Yoon, C.-C. Liu, H. Min, and F. Zhang, Quasi-one-dimensional higher-order topological insulators, arXiv:2005.14710.

[75] A. Lahiri and S. Bera, Dynamical quantum phase transitions in Weyl semimetals, Phys. Rev. B **99**, 174311 (2019).